Dissertation

Single-Cell Investigation of Endothelial Nitric Oxide Dynamics

Submitted by

Suphachai CHAROENSIN

for the Academic Degree of

Doctor of Medical Science

(Dr. scient. med.)

at the

Medical University of Graz

Institute of Molecular Biology and Biochemistry

under the Supervision of

Univ.-Prof. Mag.pharm. Dr.rer.nat. Wolfgang F. GRAIER

Assoz. Prof. Priv.-Doz. Mag.pharm. Dr.rer.nat. Roland MALLI

Univ.-Prof. Mag.pharm. Dr.rer.nat. Klaus GROSCHNER

2018

DECLARATION

Statutory declaration

I hereby declare that this dissertation is my own original work and that I have fully acknowledged by name all of those individuals and organizations that have contributed to the research for this dissertation. Due acknowledgement has been made in the text to all other material used. Throughout this dissertation and in all related publications I followed the guidelines of "Standards of Good Scientific Practice and Ombuds Committee at the Medical University of Graz".

Disclosures

Part of this thesis has been published in the following two articles:

1.) Charoensin S, Eroglu E, Opelt M, Bischof H, Madreiter-Sokolowski CT, Kirsch A, Depaoli MR, Frank S, Schrammel A, Mayer B, Waldeck-Weiermair M, Graier WF, Malli R. Intact mitochondrial Ca^{2+} uniport is essential for agonist-induced activation of endothelial nitric oxide synthase (eNOS). Free Radic Mol Med. 2017;102:248-59. Copyright 2016. Elsevier Inc.

2.) Eroglu E, Gottschalk B, Charoensin S, Blass S, Bischof H, Rost R, Madreiter-Sokolowski CT, Pelzmann B, Bernhart E, Sattler W, Hallström S, Malinski T, Waldeck-Weiermair M, Graier WF, Malli R. Development of novel FP-based probes for live-cell imaging of nitric oxide dynamics. Nat Commun. 2016;7:10623. Copyright 2016. Nature Publishing Group.

I confirm that all co-authors listed below actively contributed to the results of the thesis and the publication resulting from the thesis project. The co-authors are listed alphabetically as follows:

1.) Dr. Andrijana Kirsch, Mr. Benjamin Gottschalk, Dr. Corina T. Madreiter-Sokolowski, Dr. Emrah Eroglu, Ms. Eva Maria Bernhart, Mr. Helmut Bischof, Ms. Maria R. Depaoli, Assoc. Prof. Dr. Markus Waldeck-Weiermair, Mr. Rene Rost, Prof. Dr. Roland Malli, Ms. Sandra Blass, Prof. Dr. Saša Frank, Prof. Dr. Wolfgang F. Graier and Prof. Dr. Wolfgang Sattler
Institute of Molecular Biology and Biochemistry, Center of Molecular Medicine, Medical University of Graz

2.) Assoc. Prof. Dr. Astrid Schrammel, Prof. Dr. Bernd Mayer and Ms. Marissa Opelt
Institute of Pharmaceutical Sciences, Department of Pharmacology and Toxicology, University of Graz
3.) Dr. Brigitte Pelzmann
Institute of Biophysics, Center of Physiological Medicine, Medical University of Graz
4.) Assoc. Prof. Dr. Seth Hallström
Institute of Physiological Chemistry, Center of Physiological Medicine, Medical University of Graz
5.) Prof. Dr. Tadeusz Malinski
Nanomedical Research Laboratory, Department of Chemistry and Biochemistry, Ohio University

Furthermore, I have obtained permission to reproduce figures from the respective holders (see appendix).

1.) Figure 1.1 and 1.2 are reproduced from Zhao Y, Vanhoutte PM, Leung SW. Vascular nitric oxide: Beyond eNOS. J Pharm Sci. 2015;129(2):83-94. With permission of publisher Elsevier Inc. Copyright 2015.

2.) Figure 1.3 is reproduced from Mammucari C, Raffaello A, Vecellio Reane D, et al. Molecular structure and pathophysiological roles of the mitochondrial Ca^{2+} uniporter. Biochim Biophys Acta. 2016;1863(10):2457-64. With permission of publisher Elsevier Inc. Copyright 2016.

3.) Figure 3.1, 3.2, 3.3, 3.7, 3.8, 3.9, 3.10, 3.11 and 3.12 are reproduced from Charoensin S, Emrah E, Opelt M, et al. Intact mitochondrial Ca^{2+} uniport is essential for agonist-induced activation of endothelial nitric oxide synthase (eNOS). Free Radic Biol Med. 2017;102:248-59. With permission of publisher Elsevier Inc. Copyright 2016.

4.) Figure 3.4, 3.5 and 3.6 are reproduced from Eroglu E, Gottschalk B, Charoensin S, et al. Development of novel FP-based probes for live-cell imaging of nitric oxide dynamics. Nat Commun. 2016;7:10623. With permission of publisher Nature Publishing Group. Copyright 2016.

Graz, November 2017

ACKNOWLEDGEMENTS

This dissertation work was financially supported by Austrian Science Fund FWF (P 28529-B27). The doctoral student Mr. Suphachai Charoensin received scholarship from the University of Phayao and conference funding from the Medical University of Graz through the Doctoral School "Molecular Medicine and Inflammation".

I would like to express my sincere thanks to all people who supported me during the previous studies (M.Sc. in Biochemistry) and the present doctoral study consisting of my family, lecturers, laboratory colleagues and friends.

I could not have continued my passion in science and accomplished the higher education without kind suggestions of all three dissertation committees, including Assoc. Prof. Dr. Roland Malli and Prof. Dr. Wolfgang F. Graier from the Institute of Molecular Biology and Biochemistry, together with Prof. Dr. Klaus Groschner from the Institute of Biophysics. They were encouraging and enthusiastic in sharpening my scientific thinking and fueling my motivation to perform high-quality research.

Moreover, I would like to thank all the laboratory colleagues very much (both past and present staffs): Dr. med. Felix Karsten, Dr. Emrah Eroglu and Dr. Markus Waldeck-Weiermair for training and performing of live-cell imaging; Ms. Marissa Opelt and Dr. Andrijana Kirsch for primary cell culture and eNOS expression analysis; Dr. Rene Rost, Ms. Anna Schreilechner, Mr. Helmut Bischof, Ms. Christiane Klec, Mr. Benjamin Gottschalk, Dr. Sonja Barth and Dr. Corina T. Madreiter-Sokolowski for their excellent technical assistance and support over the period of my study stay in Graz.

TABLE OF CONTENTS

LIST OF FIGURES

LIST OF TABLES

ABBREVIATIONS

$\Delta\Psi_{mito}$	Mitochondrial membrane potential
μM	Micromolar
ADMA	Asymmetric dimethylarginine
AMP	Adenosine monophosphate
AMPK	AMP-activated protein kinase
ATP	Adenosine triphosphate
Ca^{2+}	Calcium ion
$[Ca^{2+}]_{cyto}$	Cytosolic calcium concentration
$[Ca^{2+}]_{mito}$	Mitochondrial calcium concentration
CaM	Calmodulin
cAMP	Cyclic adenosine monophosphate
cGMP	Cyclic guanosine monophosphate
CFP/YFP	Cyan/Yellow fluorescent protein
COX	Cytochrome *c* oxidase
CRAC	Ca^{2+} release-activated Ca^{2+} channel
DMEM	Dulbecco's modified eagle medium
EDHF	Endothelium-derived hyperpolarizing factor
EDRFs	Endothelium-derived relaxing factors
EGFP	Enhanced green fluorescent protein
EGTA	Ethylene glycol tetraacetic acid
EMRE	Essential MCU regulator
eNOS	Endothelial nitric oxide synthase
ER	Endoplasmic reticulum
FAD	Flavin adenine dinucleotide
FMN	Flavin adenine mononucleotide
FP	Fluorescent protein
FRET	Förster resonance energy transfer
Fura-2/AM	Fura-2 acetoxymethyl ester
geNOps	Genetically-encoded fluorescent nitric oxide probes

GPCR	G protein-coupled receptor
HUVECs	Human umbilical vein endothelial cells
IMM	Inner mitochondrial membrane
IMS	Intermembrane space
iNOS	Inducible nitric oxide synthase
$InsP_3R$	Inositol 1,4,5-trisphosphate receptor
IP_3	Inositol 1,4,5-trisphosphate
K_{Ca}	Ca^{2+}-activated potassium channels
KD	Knockdown
K_d	Dissociation constant
kDa	Kilodalton
Letm1	Leucine zipper-EF-hand containing transmembrane protein 1
MAMs	Mitochondria-associated membranes
MCU	Mitochondrial Ca^{2+} uniporter
MCUb	Mitochondrial Ca^{2+} uniporter b
MCUR1	Mitochondrial Ca^{2+} uniporter regulator 1
MICU1	Mitochondrial Ca^{2+} uptake 1
MICU2	Mitochondrial Ca^{2+} uptake 2
MLCP	Myosin light chain phosphatase
mPTP	Mitochondrial permeability transition pore
mtNOS	Mitochondrial nitric oxide synthase
NADPH	Nicotinamide adenine dinucleotide phosphate
NCX	Sodium-calcium exchanger
NCLX	Sodium-calcium-lithium exchanger
NGFI	Next generation fluorescence imaging
nM	Nanomolar
nm	Nanometer
nNOS	Neuronal nitric oxide synthase
$NO^{\bullet}$	Nitric oxide radical
$\Delta[NO^{\bullet}]_{cyto}$	Cytosolic nitric oxide differential concentration
NOS	Nitric oxide synthase

OXPHOS	Oxidative phosphorylation
PBS	Phosphate buffer saline
PI3K	Phosphoinositide 3-kinase
PKA	Protein kinase A
PKB	Protein kinase B (also known as Akt)
PKG	Protein kinase G
PLC	Phospholipase C
PMCA	Plasma membrane calcium ATPase
RFP	Red fluorescent protein
RNS	Reactive nitrogen species
ROS	Reactive oxidative species
SERCA	Sarcoplasmic/endoplasmic reticulum calcium ATPase
sGC	Soluble guanylate cyclase
shRNA	Short hairpin RNA
siRNA	Small interfering RNA
SOCE	Store-operated Ca^{2+} entry
STIM1	Stromal interacting molecule 1
TCA	Tricarboxylic acid cycle
BH_4	Tetrahydrobiopterin
TMRM	Tetramethylrhodamine methyl ester perchlorate
TRPC	Transient receptor potential canonical channels
VDAC	Voltage-dependent anion channel

ABSTRACT

Mitochondrial calcium (Ca^{2+}) uptake is a sophisticated mechanism that shapes both local and global Ca^{2+} signals, which control a variety of signaling pathways. Nevertheless, in the intact endothelial cell, it is not clear if mitochondria by taking up Ca^{2+} promote or counteract nitric oxide ($NO^{\bullet}$) synthesis, which is an essential process in vascular homeostasis. Therefore, the present study aimed to investigate the role of mitochondrial Ca^{2+} uptake on Ca^{2+}-triggered $NO^{\bullet}$ production in an immortalized endothelial cell line (EA.hy926) and respective primary human umbilical vein endothelial cells (HUVECs). For this purpose, single live-cell imaging for both $NO^{\bullet}$ and Ca^{2+} was performed using recently developed genetically-encoded fluorescent $NO^{\bullet}$ probes (geNOps) and a mitochondrial Ca^{2+} sensor (4mtD3cpv), respectively. Mitochondrial Ca^{2+} uptake is exquisitely controlled by several proteins of the inner mitochondrial membrane. So, in this study, mitochondrial Ca^{2+} uptake was manipulated using siRNAs against proteins that form the mitochondrial Ca^{2+} uniporter (MCU) complex and its associated regulatory proteins. Silencing of MCU and essential MCU regulator (EMRE) resulted in a significant decrease of mitochondrial Ca^{2+} signals and cytosolic $NO^{\bullet}$ formation in response to adenosine triphosphate (ATP)-triggered Ca^{2+} mobilization in endothelial cells. This finding was confirmed by using antimycin and oligomycin, which collapse the mitochondrial membrane potential, thereby blocking Ca^{2+} uptake by mitochondria. Down-regulation of mitochondrial Ca^{2+} uptake 1 (MICU1), a negative regulator of the MCU complex, enhanced mitochondrial Ca^{2+} uptake and Ca^{2+}-evoked $NO^{\bullet}$ formation in both cell models. In conclusion, these results indicate that the endothelial $NO^{\bullet}$ generation is indeed dependent on mitochondrial Ca^{2+} uptake. More importantly, the present study signifies a role of the MCU complex on endothelial $NO^{\bullet}$ synthase (eNOS)-mediated $NO^{\bullet}$ formation that might be a target for vascular function improvement.

ZUSAMMENFASSUNG

Die Aufnahme von Kalziumionen (Ca^{2+}) durch Mitochondrien ist ein ausgeklügelter zellulärer Prozess, welcher globale und lokale Ca^{2+} Signale beeinflusst und dadurch verschiedene Signalvorgänge in einer Zelle kontrolliert. In intakten Endothelzellen ist allerdings nicht eindeutig geklärt, ob die Aufnahme von Ca^{2+} durch Mitochondrien die Bildung von Stickstoffmonoxid ($NO^{\bullet}$) fördert oder hemmt und somit einen essentiellen Vorgang der Gefäßregulation beeinflusst. Ziel dieser Arbeit war es daher, die Rolle der Ca^{2+} Aufnahme durch Mitochondrien für die Ca^{2+}-stimulierte $NO^{\bullet}$ Produktion in einer immortalisierten Endothelzelllinie (EA.hy926) und primären Endothelzellen von der Nabelschnurrvene (HUVEC) zu untersuchen. Für diesen Zweck wurden Echtzeitmessungen von zellulären $NO^{\bullet}$ und Ca^{2+} Signalen in einzelnen Endothelzellen mit sogenannten genetisch kodierte Sensoren durchgeführt. Für zelluläre $NO^{\bullet}$ Messungen wurden die kürzlich entwickelten geNOps verwendet, während Ca^{2+} Signale in Mitochondrien mit dem sogenannten 4mtD3cpv, einem genetisch kodierten Ca^{2+} Sensor, aufgespürt wurden. Um die Aufnahme von Ca^{2+} durch Mitochondrien zu manipulieren, wurden bekannte Komponenten des Ca^{2+}-Aufnahmekomplexes (MCU Komplex) der inneren Mitochondrienmembran mittels siRNA in ihrer Expression reduziert. Eine Reduktion der Expression von MCU und EMRE, einem Regulator Protein des MCU Komplexes, führte, wie erwartet, zu einer deutlichen Verminderung der Ca^{2+} Signale in Mitochondrien sowie einer reduzierten zellulären $NO^{\bullet}$ Produktion bei Stimulierung der Endothelzellen mit Adenosintriphosphat (ATP). Dieses Ergebnis wurde mittels Oligomycin und Antimycin, welche das Membranpotential und somit die Ca^{2+}-Aufnahme der Mitochondrien aufheben, bestätigt. Die siRNA-vermittelte Reduktion der Expression von MICU1, ein Protein, welches den MCU Komplex hemmt, erhöhte Ca^{2+} Signale in Mitochondrien und die $NO^{\bullet}$ Bildung in Endothelzellen. Zusammenfassend zeigen diese Ergebnisse, dass die $NO^{\bullet}$ Biosynthese in Endothelzellen tatsächlich von der Ca^{2+} Aufnahme durch Mitochondrien positiv beeinflusst ist. Somit könnte der MCU Komplex ein wichtiger Angriffspunkt für die therapeutische Verbesserung von Gefäßfunktionen sein.

CHAPTER I

INTRODUCTION

1. Nitric oxide ($NO^{\bullet}$): biochemistry and physiological significance

$NO^{\bullet}$ is a free nitrogen radical that has various significant functions in cellular physiology (1-3). It is derived from three well-characterized protein isoforms: neuronal $NO^{\bullet}$ synthase (nNOS, NOS1) (1), inducible NOS (iNOS, NOS2) (2) and endothelial NOS (eNOS, NOS3) (3). One more isoform, which is known as a mitochondrial $NO^{\bullet}$ synthase (mtNOS), has been reported to express in hepatocytes, endothelial cells and cardiomyocytes, and it functions in Ca^{2+}-dependent manner, with mitochondrial membrane potential-sensitive property (4, 5). A synthase activity of NOS homodimer, an enzymatically-functional form, requires *L*-arginine and oxygen as substrates, nicotinamide adenine dinucleotide phosphate (NADPH) to serve as electron donor, flavin adenine dinucleotide (FAD) and flavin adenine mononucleotide (FMN) as an electron bridge, tetrahydrobiopterin (BH_4) for stabilizing coupling state, calmodulin (CaM), zinc (Zn) and iron protoporphyrin IX (haeme Fe) (Figure 1.1, right side) (6-9). In addition, NOS can be inhibited by an asymmetric dimethylarginine (ADMA, an analogue of *L*-arginine) (8, 9). Similarly, an arginase (an enzyme in urea cycle) can limit NOS activity by substrate degradation (8, 9). NOS enzyme can catalyze a formation of superoxide anion radical ($O_2^{\bullet-}$) if it is uncoupled or *L*-arginine is scarce (Figure 1.1, left side) (6-9). Except iNOS whose activity is independent of Ca^{2+}, all other isoforms require Ca^{2+}/calmodulin (CaM) complex as an enzymatic activator, thereby triggering NOS enzymatic activity (7). A number of secreted substances stimulate $NO^{\bullet}$ synthesis, such as epinephrine, serotonin, bradykinin, histamine, adiponectin and mechanical stimuli (most notably shear stress) (6, 8, 9).

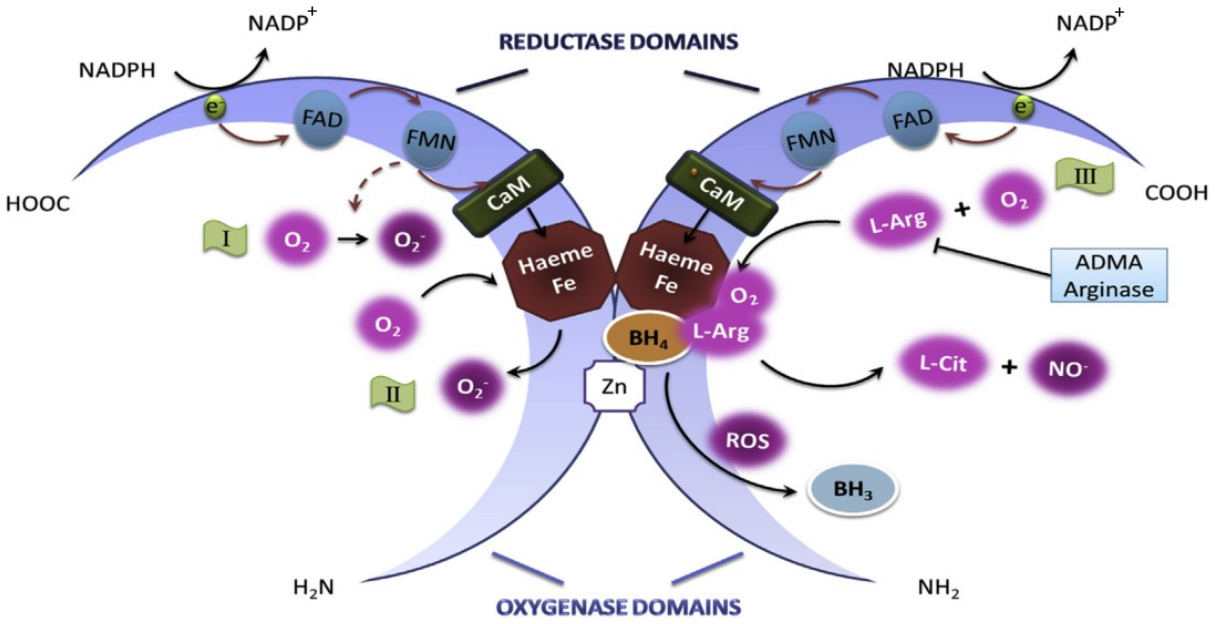

Figure 1.1 Structural organization and functional activity of NO• synthase. The enzyme consists of two identical monomers to form the functional homodimer. Each monomer has its own reductase and oxygenase domain to catalyze formation of NO•. However, on left side of the figure, a monomer (I, an uncoupled form) can produce superoxide anion radical ($O_2^{\bullet -}$) instead of NO•. A homodimer (II, a coupled form) can catalyze a formation of $O_2^{\bullet -}$ when free *L*-arginine (*L*-Arg) is lacking and the enzyme is not fully occupied by the substrate. On the right side (III), a favoring enzymatic reaction can occur when *L*-Arg and the other cofactors (Ca^{2+}/CaM, NADPH, FAD, FMN, Zn, BH_4, haeme Fe) are available at the right concentration. CaM: calmodulin, NADPH: reduced nicotinamide adenine dinucleotide phosphate, FAD: flavin adenine dinucleotide, FMN: flavin adenine mononucleotide, Zn: Zinc, BH_4: tetrahydrobiopterin, Fe: iron and $NADP^+$: oxidized nicotinamide adenine dinucleotide phosphate. [Reproduced from Zhao Y, Vanhoutte PM, Leung SW. Vascular nitric oxide: Beyond eNOS. J Pharm Sci. 2015;129(2):83-94. (6), with permission of publisher Elsevier Inc. Copyright 2015.]

Endothelium is essential in maintaining the vascular tone by releasing many biochemical substances capable of modulating the contraction and relaxation of the underlying vascular smooth muscle and regulating platelet aggregation, inflammation and thrombosis (6, 10). In vascular system, endothelium-derived $NO^{\bullet}$ has been recognized as an endogenous vascular-relaxing factor that triggers relaxation of blood vessels (10). When released from the monolayer of endothelial cells in *Tunica intima* (*Tunica mucosa*) , it liberally passes into smooth muscle cells present in *Tunica media* (*Tunica muscularis*), which is covered by *Tunica externa* (*Tunica adventitia*) (Figure 1.2) (6, 10). After reaching smooth muscle cells, it then activates a soluble guanylate cyclase (sGC), resulting in an active form that can generate cyclic guanosine monophosphate (cGMP) (11, 12). An increase in intracellular cGMP level gives rise to protein kinase G (PKG) activity; subsequently, PKG activates activity of myosin light chain phosphatase (MLCP) (8, 12). MLCP dephosphorylates an phospho-myosin; as a result, an active myosin light chain no longer exists, and the relaxation of vascular smooth muscle cells ensues (8, 12). Besides, an increment in both cGMP and PKG activity has been found to promote a re-uptake of cytoplasmic Ca^{2+} into the sarcoplasmic reticulum, a Ca^{2+} efflux and the opening of Ca^{2+}-activated potassium channels (K_{Ca}) (6). As reduced $NO^{\bullet}$-dependent vasodilation has involved in an atherosclerotic process; medically, it is used as a vasodilator in treating hypertension (13, 14) .

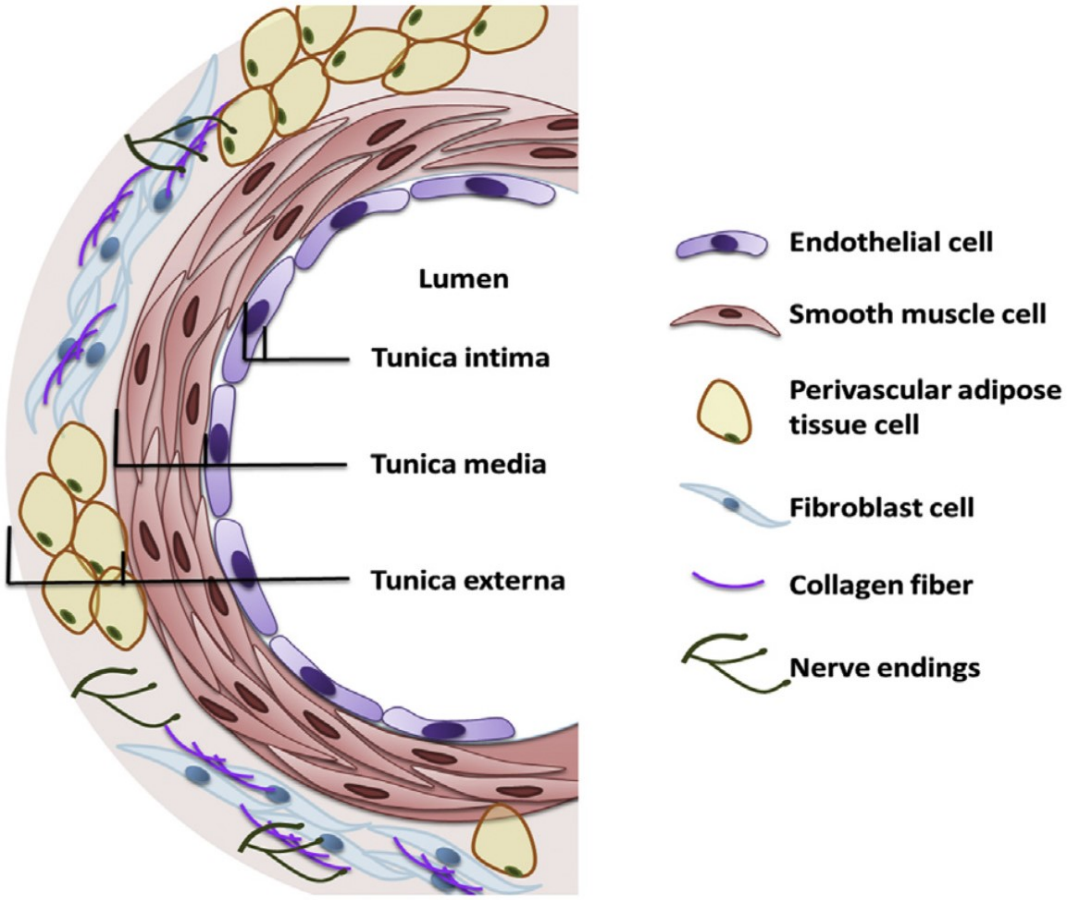

Figure 1.2 Structure of blood vessel. I. *Tunica intima* (an innermost layer) where endothelial monolayer and internal elastic membrane spread over, II. *Tunica media*, middle layer consisting of smooth muscle cell and external elastic membrane and III. *Tunica externa*, an outermost layer consisting of perivascular adipose tissue, fibroblast cell. [Reproduced from Zhao Y, Vanhoutte PM, Leung SW. Vascular nitric oxide: Beyond eNOS. J Pharm Sci. 2015;129(2):83-94. (6), with permission of publisher Elsevier Inc. Copyright 2015.]

Furthermore, a plethora of biological effects of NO• has been investigated. One of the most recognized biological functions is a signaling-metabolism coupling, allowing more oxygen to pass through *Tunica intima* of blood vessel to *Tunica media* where smooth muscle cells localize and highly energetic metabolism can occur (15-17). NO•, when passing into or formed in mitochondria, can inhibit mitochondrial respiration by competing oxygen in binding cytochrome *c* oxidase (COX) of respiratory chain complex IV (15-18). A subcellular biochemical interaction between NO• and myoglobin (hypoxic vasodilation) has also been described and proposed as a mechanistic strategy of endothelial cells to regulate oxygen consumption within smooth muscle cells, when oxygen concentration is reduced (17, 19, 20). The recent paper reveals a signaling-metabolism coupling, which has never been explained before in other cell types. It has been shown that nanomolar NO• concentrations, presumed to be within the physiological range, can reversibly increase glycolytic flux and production of lactate in astrocytes (specialized glial cells) in bicameral culture with endothelial cells (21). Upon complex IV competitive binding, protons accumulate in the mitochondrial matrix but less in intermembrane space (IMS) (15, 21). This changes proton gradient and results in altered chemical and electrical gradient (15). Therefore, mitochondrial membrane potential ($\Delta\Psi_{mito}$) becomes more positive, and voltage-dependent anion channel (VDAC) loses its functional activity (15). In addition, NO• can nitrosylate complex III and produces inhibitory effect as antimycin A (a known complex III inhibitor) can do (18, 22). As described, it is clear that the vascular relaxation is not solely the biological action of NO• in the vascular wall, but more on mitochondria-related signaling functions (6, 8, 18).

2. Principle of intracellular Ca^{2+} compartmentalization and signaling

In extracellular fluid, Ca^{2+} (2.0 - 2.6 mM) is present in three different forms: ionized, complexed to organic compounds and bound to small inorganic molecules (23). Inside a cell, total Ca^{2+} concentration, within cytosol and endoplasmic reticulum (ER), is in millimolar range (23). Nevertheless, the concentration of free Ca^{2+} ion is about 10,000-fold lower or approximately 100 nanomolar (nM) in the cytosol (23). Ca^{2+} can be complexed with inorganic compounds and organic molecules (e.g. Ca^{2+}-binding proteins), with low affinity (23, 24).

How cells maintain such a low concentration falls into two broad classes (24). The first class consists of proteins that are soluble in the cytosol (24, 25). These proteins are able to buffer Ca^{2+} to nanomolar range without modifying total concentration in the cells (25). Apart from buffering function, they can process its information when Ca^{2+}-protein complex is formed and localized spatially and temporally (23, 25). Ca^{2+} can serve as a second messenger that signals the target signaling pathways, because effector proteins (mostly enzymes) contain specific regions (binding sites) for it. When bound to target binding (regulatory) site, the enzymatic activity increases (23). A number of Ca^{2+} signals or messages are not transmitted to targets directly; alternatively, it is needed to be decoded by binding a protein called Ca^{2+} sensor especially calmodulin (CaM) (25). For example, the calmodulin-dependent kinase II (CaM kinase II) and the eNOS incorporates the calmodulin sequence within its structure (26). Calmodulin conserves Ca^{2+}'s information in the form of a conformational change that is then transmitted to the CaM kinase II and the eNOS (26, 27). Membrane-bound proteins are involved in the second class of proteins that control cellular Ca^{2+} and transport it in and out of the cells (23, 24). Likewise, these proteins allow Ca^{2+} to be accumulated between the cytosol and the lumen of two particular organelles, including mitochondria and endoplasmic reticulum; this molecular event is crucial for shaping global and local Ca^{2+} signaling (23, 24, 28, 29).

3. Endothelial purinergic signaling and vascular function

In endothelium-lining blood vessels, endothelial cells release adenosine triphosphate (ATP) in response to shear stress (viscous drag) and hypoxia (30, 31). ATP then acts as an agonist on purinergic receptors (purinoceptors) specifically P2X and P2Y; the latter is identified as a G protein-coupled receptor (32). ATP released as a cotransmitter with noradrenaline from perivascular sympathetic nerves mediates the vasoconstrictive effect upon binding P2X receptors on smooth muscle cells (33). When bound to P2Y receptors on endothelial cell surface, it leads to a phospholipase C (PLC)-β activation and an increase in inositol 1,4,5-trisphosphate (IP_3) (30). In endothelial cells, IP_3 serves as a second messenger and then mobilizes Ca^{2+} ions stored in endoplasmic reticulum upon binding inositol 1,4,5-trisphosphate receptor ($InsP_3R$) (28, 34, 35). Intracellular Ca^{2+} transiently increases and transmits its signal to respective biochemical pathways (16, 23, 36-38). $NO^{\bullet}$ synthesis by eNOS is one of the most prominent processes of endothelium, because this NOS isoform is Ca^{2+}-sensitive and needs calmodulin (27, 39, 40). Endothelial P2Y and P2X receptors mediate short-term vascular relaxation (vasodilation) under the control of cytosolic Ca^{2+} signal (33, 41). However, there is limited evidence demonstrating the correlation between mitochondrial Ca^{2+} signal and the production of this vasoactive substance.

4. Mitochondrial Ca^{2+} uniporter complex: structure and biochemical significance

The mitochondrial Ca^{2+} uniporter (MCU) and its partner proteins are a protein complex residing in an inner mitochondrial membrane (IMM) that is critical for Ca^{2+} uptake into mitochondrial matrix (28, 29, 42-44). MCU and mitochondrial Ca^{2+} exhibit fundamental roles, including 1.) shaping Ca^{2+} signaling by buffering high cytosolic Ca^{2+} (29), 2.) regulating the activity of Ca^{2+}-dependent channels (28), 3.) controlling Ca^{2+} gradients (45) and 4.) regulating mitochondrial metabolism (bioenergetics) , insulin secretion, glucose uptake/metabolism, cell survival and apoptosis (programmed cell death) (38, 43, 46-48). The mitochondrial Ca^{2+} signaling is initiated when the extramitochondrial Ca^{2+} concentration triggers the channel opening, with low activity at resting cytosolic Ca^{2+} concentration and high capacity as soon as Ca^{2+} signaling is activated (Figure 1.3) (42). The complex requires a specially-organized transport machinery for Ca^{2+} uptake and sequestration. Table 1.1 shows the list of inner

mitochondrial proteins that make up the Ca^{2+} uniporter complex. Each protein is described in detail in 4.1-4.4.

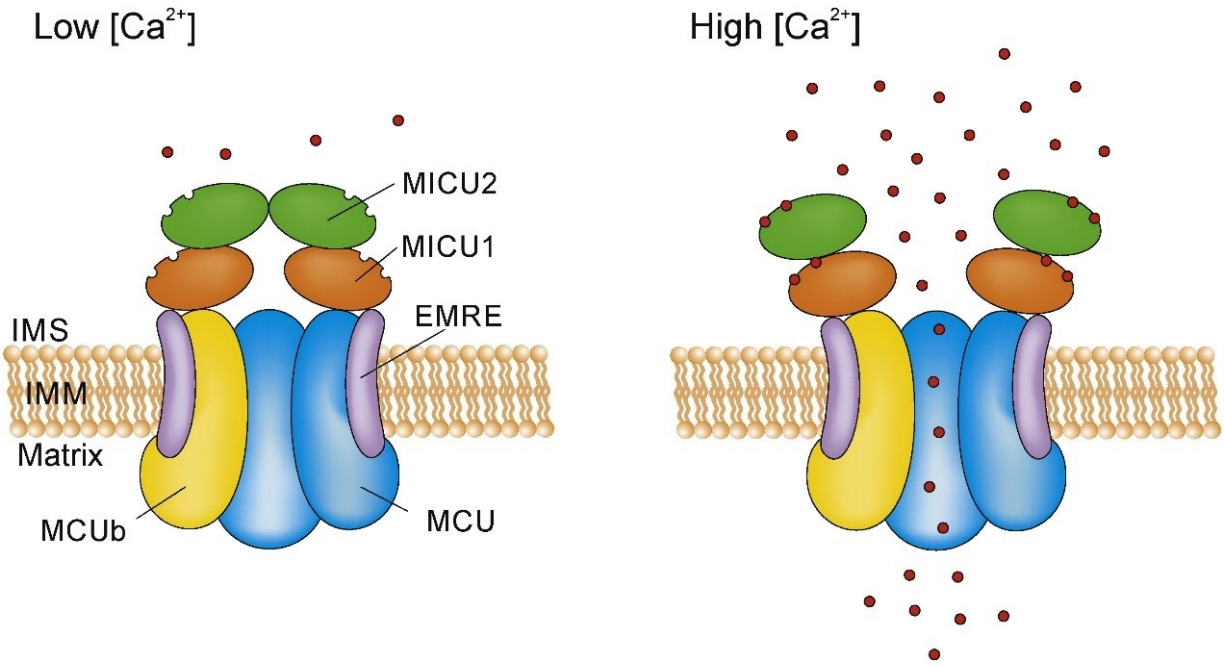

Figure 1.3 Mitochondrial Ca^{2+} uniporter complex. The complex is incorporated by the assemble of a mitochondrial Ca^{2+} uniporter (MCU), an essential MCU regulator **(**EMRE**)**, a mitochondrial Ca^{2+} uptake 1/2 (MICU1/2), a mitochondrial Ca^{2+} uniporter b (MCUb), an inner mitochondrial membrane (IMM) and an intermembrane space (IMS). Mitochondrial Ca^{2+} uniporter regulator 1 is not depicted here. [Reproduced from Mammucari C, Raffaello A, Vecellio Reane D, et al. Molecular structure and pathophysiological roles of the mitochondrial Ca^{2+} uniporter. Biochim Biophys Acta. 2016;1863(10):2457-64. (42), with permission of publisher Elsevier Inc. Copyright 2016.]

Table 1.1 Core components of mitochondrial Ca^{2+} uniporter complex and associated proteins

Inner mitochondrial membrane proteins	Molecular weight (kDa)	Function or interaction with the other complex proteins
Mitochondrial Ca^{2+} uniporter (MCU)	40	Pore-forming subunit of the uniporter (49, 50)
Essential MCU regulator (EMRE)	10	Coordinator protein for an interaction of MCU with MICU1/MICU2 (51)
Mitochondrial Ca^{2+} uniporter regulator 1 (MCUR1)	40	Interacts with MCU but not with MICU1 (44, 52)
Mitochondrial Ca^{2+} uptake 1 (MICU1)	50	Interacts with MCU and sets a threshold for Ca^{2+} entering mitochondria Maintains low matrix Ca^{2+} level (approximately100 nM) (43, 53)
Mitochondrial Ca^{2+} uptake 2 (MICU2)	45	Associates with the MICU1/MCU complex (54)
Mitochondrial Ca^{2+} uniporter b (MCUb)	40	Paralog of MCU (a dominant-negative subunit) (55)

Mitochondria conduct the rapid Ca^{2+} transport across inner and outer membranes and sequester it in the matrix, thereby buffering dramatical rise of intracellular Ca^{2+} during endoplasmic reticulum Ca^{2+} release and extracellular influx (29, 56). The mitochondrial membrane potential created by electrochemical gradient across inner mitochondrial membrane plays a critical role as a driving force of Ca^{2+} uptake (57). By pumping protons (H^+) towards the intermembrane space, mitochondria generate a voltage of -180 mV inside the matrix (57). To prevent Ca^{2+} overload that could cause detrimental effect to the cell, mitochondria release Ca^{2+} via ion exchangers (antiporters) by exchanging Ca^{2+} with sodium (Na^+) or H^+ (58, 59). In 2009, Jiang and coworkers identified a leucine zipper-EF-hand containing transmembrane protein 1 (Letm1) as the Ca^{2+}/H^+ antiporter (60). Letm1 is believed to conduct Ca^{2+} extrusion especially when the mitochondrial Ca^{2+} concentration is increased in the matrix (60). Moreover, Letm1 has also been reported to maintain mitochondrial potassium (K^+) levels by exchanging H^+ (61). In 2010, the mitochondrial Na^+/Ca^{2+} exchanger (NCLX) has been discovered by Palty and colleagues. This emphasizes the fundamental knowledge that mitochondrial Na^+/Ca^{2+} antiport is electrogenic and responsible for exchanging three Na^+ ions per one Ca^{2+} ion to maintain low mitochondrial Ca^{2+} concentration (62).

One of the key properties of the MCU is to maintain a low apparent Ca^{2+} affinity under physiological conditions and to allow massive amounts of Ca^{2+} to rush in the mitochondrial matrix under stimulations (29, 56, 63). As the endoplasmic reticulum is the major intracellular Ca^{2+} store, it has been found to form a microdomain with mitochondria in a close vicinity, the so called mitochondria-associated membranes (MAMs) (64, 65). After inositol trisphosphate-stimulated intracellular Ca^{2+} release, the MAMs with high Ca^{2+} concentration can transiently establish a close apposition between the mitochondria (VDAC and MCU as Ca^{2+} uptake channel) and the endoplasmic reticulum (inositol trisphosphate receptor as a Ca^{2+} release channel) (65). The communication between these two organelles is pivotal for intracellular and mitochondrial Ca^{2+} signaling. Therefore, upon formation of MAMs, the sophisticated mitochondrial Ca^{2+} uptake mechanism ensures an instantaneous Ca^{2+} accumulation within mitochondrial matrix, thereby buffering and shaping Ca^{2+} signaling and maintaining appropriate biochemical reactions and cellular homeostasis (65).

4.1 Mitochondrial Ca^{2+} uniporter (MCU) and its paralog MCUb

MCU is well-recognized as a pore-forming subunit of the MCU complex with a highly-selective low conductance (49). The nuclear MCU gene, which is located on chromosome 10, encodes a 40 kDa protein that loses its cleavable target sequence during mitochondrial import, resulting in an actual 35 kDa mature form (49, 50). MCU oligomerizes in the mitochondrial inner membrane as part of a larger complex at an apparent molecular weight of 480 kDa (1, 55). Thus, the uniporter complex includes different regulatory subunits (Figure 1.3), and one of these subunits is represented by the MICU1, which is required for agonist-mediated Ca^{2+} uptake into mitochondria (43, 53). The molecular understanding of the structure and function of the MCU complex is now highlighting the pleiotropic role of mitochondrial Ca^{2+} signals (42, 66). Between 2010 and 2017, MCU function has been extensively investigated. It has been reported that MCU-mediated mitochondrial Ca^{2+} uptake matches energetic supply and ATP production (46), buffers cytosolic Ca^{2+} transients (34), regulates cell survival and death (43, 48), controls skeletal muscle trophism (67) and regulates breast cancer progression via hypoxia-inducible factor-1α (HIF-1α)(68). In addition, the study conducted in pancreatic beta cells shows that mitochondrial Ca^{2+} uptake via the MCU complex contributes to sustained insulin release by accelerating ATP synthesis (69). Recently, in 2017, MCU (Cys97 residue) acts as a redox sensor that increases MCU activity in response to oxidative stress, thereby causing Ca^{2+} overload (70).

Unlike MCU, MCUb is a dominant-negative subunit in the multimeric channel. It cannot assemble and function as a Ca^{2+}-permeable channel but can negatively regulate MCU complex (55). Accordingly, it contributes to the spatiotemporal control of mitochondrial Ca^{2+} uptake and sets a maximal mitochondrial Ca^{2+} carrying capacity of each cell types (71).

4.2 Essential MCU regulator (EMRE)

Essential MCU regulator or EMRE, as the name indicated, is the essential MCU-regulating protein constituting the MCU complex. EMRE is a 10 kDa protein, which is rich in aspartate residues, and spans the inner mitochondrial membrane (51). It facilitates an establishment of Ca^{2+} channel activity by connecting MICU1/MICU2 dimer to MCU (51). Absence of EMRE expression could abolish Ca^{2+} uptake ability by mitochondria *in vivo*, and MCU ablation impairs EMRE protein stability (51, 72). A new study from Vais and colleagues reveals that EMRE is not required only for efficient assemble of the MCU complex but also

for sensing of matrix Ca^{2+} from which a gatekeeping property of the MCU is regulated (73). Regulatory function of EMRE on MCU channel activity is understood in the way how mitochondria can protect themselves from Ca^{2+} depletion and overload by sensing Ca^{2+} on both sides of the inner mitochondrial membrane (73). This molecular mechanism requires the cytoplasmic Ca^{2+} and the key MCU-associated regulators, including MICU1 and MICU2 (63).

4.3 Mitochondrial Ca^{2+} uptake 1 and 2 (MICU1 and MICU2)

MICU1 and MICU2 are the key MCU-associated regulators (43, 53, 54, 74). MICU1 is a 54 kDa inner mitochondrial membrane protein containing two highly-conserved EF-hand Ca^{2+}-binding domains (53). In 2012, regulatory function of MICU1 on mitochondrial Ca^{2+} uptake was revealed. Mallilankaraman and colleagues proposed an essential role for MICU1 as a gatekeeper for MCU-mediated Ca^{2+} accumulation, preventing an *in vivo* mitochondrial Ca^{2+} overload (43). In opposition to previous report, MICU1 silencing shows no change in mitochondrial Ca^{2+} uptake capacity but promotes basal mitochondrial Ca^{2+} accumulation (43). When MICU1 gene is down-regulated, the mitochondria become constitutively loaded with Ca^{2+}; therefore, MICU1 sets the threshold for Ca^{2+} entry through MCU when the intracellular Ca^{2+} concentration is maintained under resting conditions (43, 75). However, the contrast has been reported that the down-regulation of MICU1 reduces the mitochondrial Ca^{2+} level in EF-hand-dependent manner without impairing mitochondrial respiration or membrane potential (53). An in-depth investigation reveals more on MCU-MICU1 interaction that MICU1 stabilizes the closed state of the MCU complex (43, 75). It limits mitochondrial Ca^{2+} entry under resting conditions or during tiny cytosolic Ca^{2+} increases through a mechanism that requires its Ca^{2+}-binding EF-hand domains (43, 75). A recent publication by Waldeck-Weiermair and colleagues points out that the cytosolic Ca^{2+} elevation rearranges MICU1 multimers, resulting in the activation of mitochondrial Ca^{2+} uptake (76). This study precisely clarifies how conformational change prompts MICU1 function, and it also leads to a conclusion that MICU1 rearrangement requires the EF-hand motifs and correlates with cytosolic Ca^{2+} transients (76). Thus, it confirms the principle of mitochondrial Ca^{2+} uptake to which MICU1 cooperates with MCU to allow Ca^{2+} sequestration inside the mitochondrial matrix (43, 75).

MICU2, a homolog of MICU1, is another MCU-associated regulator that acts as an inhibitor of MCU when the cytosolic Ca^{2+} is low (54). An inhibitory effect disappears during

intracellular Ca^{2+} rise (above 7 μM), whereas MICU1 activates Ca^{2+} channeling activity of MCU at cytosolic Ca^{2+} above 2.5 μM (54). Unlike MICU2, MICU1 has been demonstrated a double role over MCU regulation depending on cytosolic Ca^{2+} concentration, inhibitory at low concentration and activatory at high concentration (74). These opposite affinities to Ca^{2+} of both MICU1 and MICU2 tune MCU activity to ensure Ca^{2+} uptake, buffering and signaling (74).

4.4 Mitochondrial Ca^{2+} uniporter regulator 1 (MCUR1)

MCUR1 is an integral component of the mitochondrial Ca^{2+} uptake machinery, with two transmembrane α-helices (52). It has been reported to be an important regulator of MCU-dependent mitochondrial Ca^{2+} uptake by interacting with MCU to mediate uniporter activity and to biochemically regulate cellular metabolism (44, 77). It regulates MCU-mediated Ca^{2+} uptake driven by mitochondrial membrane potential (44, 52). MCUR1 knockdown revokes Ca^{2+} uptake by mitochondria in both intact and permeabilized cells and disrupts oxidative phosphorylation (77). Even though it is well-described scientifically, a recent conversed proposal against the above conclusions is raised; that is, downregulation of MCUR1 produces a specific cytochrome *c* oxidase assembly defect (78). This molecular event results in a reduced mitochondrial membrane potential, due to less proton gradient across inner membrane; consequently, mitochondrial Ca^{2+} uptake decreases (78). This conclusion is opposed to Mallilankaraman's paper by pronouncing that Ca^{2+} transport across inner membrane of mitochondria is a secondary effect according to a defective cytochrome *c* oxidase assembly that leads to a reduction in mitochondrial membrane voltage (78). A clarity to this discrepancy has partially solved in a following year. In 2016, Tomar and colleagues showed that MCUR1 was essential for MCU complex function, since it serves as a scaffold factor and promotes mitochondrial respiration (79).

4.5 Uncoupling protein 2 and 3 (UCP2/3)

UCP2 and UCP3 are in the superfamily of mitochondrial ion transporters that are embedded in the mitochondrial inner membrane (80). Trenker and co-workers have demonstrated that these two proteins are essential for mitochondrial Ca^{2+} sequestration in response to cell stimulation (81). Both UCP2 and UCP3 fundamentally involve in the uptake of Ca^{2+} that is released from internal store (82). UCP3 can also tune mitochondrial Ca^{2+} uptake

depending on its site on intermembrane loop 2 (83). Recently, it has been reported that UCP2 exhibits its regulatory role in modulating the MCU-dependent Ca^{2+} uptake into mitochondria (84).

5. Endothelial Ca^{2+} signaling and eNOS functionality

The precise regulation of cytoplasmic Ca^{2+} within endothelial cells is important for the control of vascular tone (85). The functional activity of the cells especially their abilities to produce $NO^{\bullet}$ depends on cytosolic Ca^{2+} level (27). Normally, the endothelial cytosolic Ca^{2+} concentration is maintained at very low level, approximately 100 nM, but it can be increased via agonist-mediated endoplasmic reticulum Ca^{2+} release and extracellular Ca^{2+} entry (34, 37). In addition, the plasma membrane potential and the activity of membrane-bound channels (e.g. voltage-gated Ca^{2+} channels and Ca^{2+}-activated K^{+} channels) are crucial for controlling cellular Ca^{2+} homeostasis (23, 57).

Endothelial cells, in contrast to smooth muscle cells, are non-excitable cells to which intracellular Ca^{2+} serves as a key regulator of their functions, including the production and release of endothelium-derived relaxing factors (EDRFs), such as $NO^{\bullet}$, prostacyclin, von Willebrand factor (vWF) and endothelium-derived hyperpolarizing factor (EDHF) (86, 87). These mediators play pivotal roles in regulating vascular relaxation (86-88). Regarding endothelial cell physiology, the alterations in intracellular Ca^{2+} concentration are generated in response to agonist-mediated receptor activation (e.g. purinergic, cholinergic and adrenergic receptors) and in response to mechanical stimulus, most influentially a shear stress (3 , 9) . Augments in cytosolic Ca^{2+} concentration are biphasic, meaning that an initial phase of Ca^{2+} release from endoplasmic reticulum is followed by the extracellular Ca^{2+} entry (34). It has been well-understood that ATP (an endogenous IP_3-generating agonist) , when bound to purinergic receptor preferentially P_2Y subtype, can increase intracellular Ca^{2+} by activating both Ca^{2+} release from endoplasmic reticulum and Ca^{2+} influx from the extracellular fluid (28, 34, 89). Apart from the IP_3, histamine, a known endogenous inflammatory mediator, can produce similar effect (34, 90). Moreover, the study shows that it causes a release of nicotinic acid adenine dinucleotide phosphate (NAADP) , an intracellular second messenger, that can mobilize Ca^{2+} from the internal store (90).

The elevation of cytosolic Ca^{2+} in endothelial cells is associated with the hyperpolarization caused by the activation of Ca^{2+}-activated K^+ channels (86, 87). The endothelial hyperpolarization constitutes a mechanism for extracellular Ca^{2+} entry as the driving force for Ca^{2+} is enhanced (87). The IP_3-induced depletion of Ca^{2+} within endoplasmic reticulum via IP_3 receptor ($InsP_3R$) or blockade of sarcoplasmic reticulum (SERCA) both SERCA2b and SERCA3 promotes the cytosolic Ca^{2+} increase via store-operated Ca^{2+} release-activated Ca^{2+} (CRAC) channels (28, 91, 92). Afterwards, the activation of stromal interaction molecule 1 (STIM1) and Ca^{2+} release-activated Ca^{2+} channel protein 1 (Orai1) is engaged to mediate endoplasmic reticulum Ca^{2+} refilling (34, 91). Recently, it has been demonstrated that an endothelial endoplasmic reticulum Ca^{2+} refilling through nanojunctions is mediated by the simultaneous Na^+ / Ca^{2+} exchanger and Orai channel function (35). Besides, as present on plasma membrane of endothelial cells, the transient receptor potential canonical (TRPC) channels play a major role in shear stress-mediated endothelium-dependent dilation (93). Shear stress created on endothelial monolayer triggers endoplasmic reticulum Ca^{2+} release and PKB (Akt) activation (94). After stimulation of Ca^{2+} release is over, the TRPC channels are immediately inactivated (93). This inactivation decreases Ca^{2+} entry by pumping Ca^{2+} out of the cell by plasma membrane Ca^{2+} ATPase (PMCA) (93).

6. Regulation of endothelial $NO^{\bullet}$ synthase activation

eNOS function is activated by the Ca^{2+} signals triggered by several agonist-receptor stimulations. Post-translational modification mediated by several kinase pathways is the key mechanism that alters phosphorylation state of eNOS and its enzymatic activity (3, 8, 9, 13, 23, 26, 27).

6.1 Ca^{2+}/calmodulin-dependent eNOS activation and $NO^{\bullet}$ production: a role of agonist/receptor-mediated intracellular Ca^{2+} signaling

There are numerous endogenous agonists that can alter Ca^{2+} concentration and dynamics in endothelial cells (7, 23, 26, 27). When agonists bind to and activate specific plasma membrane receptors, an increase in the intracellular Ca^{2+} concentration activates eNOS activity via several signaling pathways (15, 26, 27, 89). Most endothelial plasma membrane receptors are coupled to the downstream signaling cascades, and they are linked to specific guanine nucleotide-binding proteins (G proteins) (26, 89). Plasma membrane receptors can

respond to certain agonists; catecholamines (e.g. acetylcholine) and serotonin are coupled to the activation of eNOS by G_i (G inhibitory) protein (8). On the other hand, adenine nucleotides (particularly ATP) and bradykinin have G_q protein coupling (89). The G proteins are coupled to phospholipase C that can result in an increase of IP_3 (23, 57). Elevated IP_3 binds its receptor and triggers Ca^{2+} release (23, 34). Apart from this receptor activation, B2-bradykinin activates ADP-ribosyl cyclase - an enzyme capable of catalyzing the formation of cyclic ADP-ribose (95). In human mesenteric artery endothelial cells but not in EA.hy 926 cells, the cyclic ADP-ribose enhances caffeine-induced Ca^{2+} release via ryanodine receptor 3 (RyR3) (95, 96). When mitochondrial Ca^{2+} uptake occurs via MCU complex, the rhythmic Ca^{2+} release from mitochondria (via Na^+/Ca^{2+} exchanger) creates Ca^{2+} oscillation signals that can contribute to the balanced Ca^{2+}-dependent eNOS activation (26, 27, 85). During the intracellular release, free Ca^{2+} seeks its way to calmodulin, thereby forming Ca^{2+}/ CaM complex (25, 27). This complex further binds its conserved domain located on eNOS (6, 9). Upon binding, it facilitates the electron flux from the reductase to the oxygenase domain (6, 9). Notably, it is also able to activate post-translational modification (eNOS phosphorylation) via Ca^{2+}-dependent kinase pathways (9, 26, 27).

6.2 Post-translational modification of eNOS by phosphorylation

The phosphorylation of specific serine, threonine and tyrosine residues of eNOS is the conserved regulation of enzymatic activity for endothelial cells across species. (10, 97). Phosphorylation of eNOS at different amino acid residues (hotspots) results in either negative (inhibitory) or positive (stimulatory) effect (9, 10, 97, 98). The important effector proteins comprise of cAMP-dependent PKA, AMP-activated protein kinase (AMPK), CaM kinase II and phosphoinositide 3-kinase (PI3K)/PKB (8, 9, 26, 27, 98-100). Phosphorylation at different tyrosine residues modulates enzymatic activity (8, 9). PKA, AMPK and CaM kinase II activate eNOS by phosphorylating Ser1177 (human) (26, 27). Similarly, PKB phosphorylates eNOS at Ser1177 and Ser1179 (bovine), thereby stimulating enzyme activity at low cytosolic Ca^{2+} level (9, 94). On the contrary, Thr495 phosphorylation by protein kinase C results in the attenuated enzyme activity (98, 100). Phosphorylation at Tyr657 by proline-rich tyrosine kinase (stimulation by insulin, shear stress, angiotensin II, or hydrogen peroxide) leads to declined eNOS activity (39, 98-100). This post-translational process then induces a negative feedback to balance cellular $NO^{\bullet}$ level and prevents tetrahydrobiopterin depletion as well as

eNOS uncoupling (10, 39). Notably, eNOS perturbation has been implicated in endothelial dysfunction and vascular disease; hence, exploring how to enhance the enzyme function might be a promising therapeutic strategy for such disease (6, 9, 10, 98).

7. Rationale and research question

Mitochondrial Ca^{2+} uptake is essential for cytosolic Ca^{2+} signaling, metabolism, bioenergetics, cell survival and activation of cell death (apoptosis) in various cell types, including endothelial cells (29, 43, 46, 48, 56, 63, 72, 79). Endothelial mitochondria participate in cytosolic Ca^{2+} phenotype through rapid Ca^{2+} buffering, thereby shaping global and local Ca^{2+} signaling (34, 37, 56, 65). Concomitantly, the Ca^{2+} signaling in this multifunctional organelle is considered as the mitochondrial Ca^{2+} signaling (34, 37, 56). Furthermore, cytosolic Ca^{2+}-dependent biochemical reactions proceed in the appropriate directions (34, 37, 56). Endothelial Ca^{2+} concentration is maintained in resting condition (34, 85). However, under agonist- or shear stress-induced intracellular Ca^{2+} mobilization, an augmented Ca^{2+} concentration is able to govern a key function of endothelium, the production of $NO^{\bullet}$ (a potent vasodilator) (34, 85). In the past, there is an attempt to investigate whether mitochondrial Ca^{2+} uptake is associated with endothelial $NO^{\bullet}$ synthesis using permeabilized calf pulmonary artery endothelial cells (5, 101). Nevertheless, a physiological property of some membrane-bound proteins as well as an accumulation of fluorescent dye might be interfered during permeabilization (102). This research gap raises the question on the actual role of mitochondrial Ca^{2+} signals on $NO^{\bullet}$ formation in intact endothelial cells. Therefore, manipulating mitochondrial Ca^{2+} uptake based on the recently-identified MCU-mediated Ca^{2+} uptake is more physiological and less deleterious to the cells (102). To perform $NO^{\bullet}$ imaging in living cells, a conventional synthetic fluorescent dye called 4,5-diaminofluorescein diacetate (DAF-2-DA) has been frequently used with some inherent pitfalls (102, 103). It senses $NO^{\bullet}$ metabolites, including nitrite and nitrate; in other words, it indirectly reflects the amount of $NO^{\bullet}$ within the cells (102, 103). Utilizing a more direct, real-time method to visualize $NO^{\bullet}$ dynamics in living cells is challenging to overcome all these pitfalls. Thanks to the innovative technology in $NO^{\bullet}$ imaging introduced in 2016 by Eroglu and colleagues, the novel sensor called genetically-encoded $NO^{\bullet}$ probes (geNOps), which can rapidly sense $NO^{\bullet}$ radical produced by endothelial cells in real-time (104, 105). Overall, the output of this thesis

will advance the current knowledge regarding how MCU complex-mediated mitochondrial Ca^{2+} uptake associates with endothelial $NO^{\bullet}$ synthesis. Moreover, it might provide a new strategy for harnessing $NO^{\bullet}$ production in the endothelium and improving vascular function.

8. Research purposes

8.1 To study a role of MCU complex on endothelial $NO^{\bullet}$ synthesis using small interfering RNA technology for genetic manipulation and the novel genetically-encoded $NO^{\bullet}$ probe

8.2 To investigate the production of $NO^{\bullet}$ using pharmacological tools against mitochondrial bioenergetics

9. Research outcome: perspective on health relevance

By investigating the functional role of mitochondria on endothelial cell function, the results of this thesis might lead the way for further high-level study regarding vascular health. As it is highlighted in this thesis that MCU complex is crucial for $NO^{\bullet}$ biochemistry *in vitro*, it is worth designing *in vivo* experimental protocol to learn how pathophysiological animal model system (e.g. vascular dysfunction) manifests if the targeted endothelial MCU complex genes are manipulated. This MCU complex characterization will possibly unveil a new therapeutic target in improving vascular function.

CHAPTER 2

MATERIALS AND METHODS

2.1 Chemicals

Chemicals used in the solution preparations, cell cultures, transfections and treatments are analytical grade or higher (Table 2.1, in alphabetical order).

Table 2.1 Chemicals, probes and antibodies

Names of chemicals and antibodies	Source	Biological role or purpose of use
Adenosine triphosphate (ATP)	Roth	IP_3-generating agonist
Antimycin	Sigma	Selective, respiratory chain complex III competitive inhibitor
BacMam 4mtD3cpv virus (mitochondrial cameleon)	Life Technologies	Mitochondrial Ca^{2+} imaging in HUVECs
β-actin	Sigma	Internal control of Western blot analysis
Dulbecco's modified Eagle's medium (DMEM)	Sigma	Nutrient support of cell growth and proliferation
ECL detection reagent	Biozym Scientific	Protein chemiluminescence
Endothelial basal medium (EBM)	Lonza	HUVECs culture
Endothelial growth medium (EGM)	Lonza	HUVECs culture
eNOS, phospho-eNOS (pS1177) and anti-mouse IgG secondary antibody	BD Transduction Laboratories	For detecting expression level of eNOS and phospho-eNOS
eNOS-RFP	Addgene	eNOS overexpression in HEK293
Fura-2-acetoxymethyl ester (Fura-2/AM)	Invitrogen	Cytosolic Ca^{2+} fluorescent dye
C/G-geNOp, mtC/mtG-geNOp, C/G-geNOp^{mut} and mtC/mtG-geNOp^{mut}	NGFI	$NO^{\bullet}$-sensitive probe for live-cell imaging
MitoTracker™ Red CMXRos	Invitrogen	Mitochondrial marker

Names of chemicals and antibodies	Source	Biological role or purpose of use
N^{ω}-Nitro-L-arginine methyl ester hydrochloride (L-NAME)	Sigma	NOS inhibitor
L-N^{G}-nitro arginine	Sigma	NOS inhibitor
Oligomycin	Sigma	Selective, F_1/F_0 ATP synthase competitive inhibitor
Tetramethylrhodamine methyl ester perchlorate (TMRM)	Invitrogen	Mitochondrial membrane potential fluorescent dye
TransFast™ (cationic liposome-based transfection reagent)	Promega	Plasmid or siRNA delivery

2.2 Cell culture

Both human umbilical vein endothelial cells (HUVECs) and its surrogate cell line (EA.hy926) were used in the key experiments to investigate the role of mitochondrial Ca^{2+} uptake on eNOS-derived $NO^{\bullet}$ production (106). According to the company's protocol (Lonza, Basel, Switzerland), HUVECs were cultured maximally 14 days and then were seeded onto 1% gelatin-coated plate for further experiments. They were cultured in endothelial basal medium (EBM) in the presence of endothelial growth medium (EGM) and growth factors in a humidified incubator at 37°C and 5% CO_2. EA.hy926 cells were grown in DMEM medium containing 1% HAT (5 mM hypoxanthine, 20 μM aminopterin, 0.8 mM thymidine), 10% fetal bovine serum, 100 U/ml penicillin, and 100 μg/ml streptomycin at 37°C and 5% CO_2 (34, 76, 104). eNOS-RFP expressing human embryonic kidney cells (HEK293) were also used in comparing the effect of mitochondrial Ca^{2+} uptake on $NO^{\bullet}$ formation. They were cultured in DMEM medium supplemented with 10% fetal bovine serum and were maintained at 37°C and 5% CO_2 (104). HeLaS3 cells were cultured using the same condition as HEK293 cells and used in colocalization of mitochondrial nitric oxide probe. EA.hy926, HeLaS3 and HEK293 cells were plated onto 30 mm glass cover slips for 24-48 hours prior to transfections.

2.3 Transient gene silencing and fluorescent protein (FP)-tagged constructs for live-cell imaging

Small interfering RNA (siRNA) technology is an effective tool to transiently knockdown the expression of gene of interest. It was applied in genetic manipulation of

mitochondrial Ca^{2+} uptake machinery, including MCU, EMRE and MICU1. The sequence of each siRNA as well as the scrambled siRNA for negative control used in this study were represented in the table 2.2. All siRNAs were from Microsynth (Balgach, Switzerland) and kept in refrigerator (4°C). Scrambled siRNA was used as a control and it could not target any known genes in the cell; we could distinguish sequence-specific silencing from non-specific effects. When delivered into target cells, siRNAs, except scrambled siRNA, binds their specific complementary sequence present of messenger RNA and induces a multiprotein complex called RNA-induced silencing complex (RISC) to degrade respective mRNA. The efficiency of gene knockdown can be monitored after 48 - 96 hours following transfection.

Förster resonance energy transfer (FRET)-based mitochondrial Ca^{2+} sensor 4mtD3cpv (mt-cameleon) was from Prof. Dr. Roger Tsien (107). Green fluorescent protein fused-genetically encoded $NO^{\bullet}$ probe in the form of G-geNOp plasmid was introduced to all tested cells used in the present study to investigate the effect of MCU-mediated mitochondrial Ca^{2+} uptake on $NO^{\bullet}$ dynamics prior to or during ATP-evoked endoplasmic reticulum Ca^{2+} release and store operated Ca^{2+} entry (104).

Table 2.2 siRNAs

siRNAs	Nucleotide sequence (5´–3´)
scrambled siRNA (negative control)	UUCUCCGAACGUGUCACGU
hMCU-si1	GCCAGAGACAGACAAUACU
hMCU-si2	GGAAAGGGAGCUUAUUGAA
hEMRE-si	GAACUUUGCUGCUCUACUU
hMICU1-si1	GCAGCUCAAGAAGCACUUCAA
hMICU1-si2	GCAAUGGCGAACUGAGCAAUA

2.4 Cell transfections and adenoviral transductions

For transient transfection of probe, plasmid DNAs and siRNAs, TransFast™ transfection reagent (cationic liposome) was prepared and used according to the manufacture's instruction.

2.4.1 Co-transfection of plasmid DNAs and siRNAs

Co-transfection protocol was modified from Waldeck-Weiermair et al. (76). EA.hy926 cells on glass cover slips in six-well plates (at 60-70% confluence) were washed with phosphate-buffered saline (PBS) and then co-transfected with either 100 nM of the respective siRNA (s) or scrambled siRNA and 1.5 μg of the plasmid coding either for G-geNOp or for G-geNOp^{mut} (negative control) in the presence of 3 μL of TransFast™ and transfection medium (serum- and antibiotic-free DMEM) (76, 108). For mitochondrial Ca^{2+} imaging, mitochondrial cameleon 4mtD3cpv was co-transfected together with respective siRNA (s). To express the endothelial NO$^{\bullet}$ synthase C-terminally fused to a red fluorescent protein (eNOS-RFP) in HEK293 cells, 2.5 μg of eNOS-RFP was added into transfection medium containing the respective siRNA (s) and G-geNOp (104). After overnight incubation in humidified incubator (37°C and 5% CO_2), the transfection mixture was removed, and the cells were further maintained in DMEM medium. The experiments were performed 42-54 hours after transfection. For visualizations of NO$^{\bullet}$ dynamics in the absence of gene silencing, EA.hy926 cells were transfected with 1.5 μg of G-geNOp. C-geNOp and mtG-geNOp or G-geNOp and mtC-geNOp were introduced to EA.hy926 cells (1.5 μg each) for co-imaging purpose.

2.4.2 Adenoviral transductions

For mitochondrial Ca^{2+} visualizations, EA.hy926 cells and HUVECs at 50-60% confluence were infected with BacMam 4mtD3cpv virus. HUVECs at the same confluence were infected with G-geNOp adenovirus for cytosolic NO$^{\bullet}$ imaging. After incubation, the infected cells were transiently transfected with respective siRNA (s) (76, 104, 109).

2.5 Buffer solutions

Before imaging, cells were washed and incubated in a storage buffer containing NaCl (138 mM), $CaCl_2$ (2 mM), KCl (5 mM), $MgCl_2$ (1 mM), HEPES (1 mM), $NaHCO_3$ (2.6 mM), KH_2PO_4 (0.44 mM), Na_2HPO_4 (0.34 mM), D-glucose (10 mM), vitamin mixture (0.1%), essential amino acid mixture (0.2%) and penicillin/streptomycin (1%), pH 7.44. Experimental

buffer (EB-buffer) (HEPES buffer) with or without Ca^{2+} was mainly used throughout the imaging (76, 110). It composes of NaCl (145 mM), $CaCl_2$ (2 mM) or EGTA (1 mM), KCl (5 mM), $MgCl_2$ (1 mM), HEPES (10 mM) and D-glucose (10 mM), pH 7.44. ATP (100 μM) was added to respective buffers for mobilizing Ca^{2+} from endoplasmic reticulum. Antimycin (5 μM) and oligomycin (1 μM) were mixed in the respective buffers to inhibit mitochondrial complex III and ATP synthase, respectively (5, 101). These two compounds cause the mitochondrial bioenergetic collapse and the subsequent dissipated mitochondrial membrane potential and interfered mitochondrial Ca^{2+} uptake (34, 36). HEPES buffer containing ferrous fumarate (1 mM) and ascorbic acid (1 mM) (iron buffer) was prepared freshly for $NO^{\bullet}$ imaging (104).

2.6 Cytosolic and mitochondrial Ca^{2+} imaging

2.6.1 Fura-2 measurements

Fura-2/AM is the synthetic, cell-permeant fluorescent Ca^{2+} indicator (111). After hydrolysis of esterified methyl, the dye accumulates within the cytosol and lasts for a long period of time. Fura-2 allows a ratiometric Ca^{2+} imaging (K_d = 0.224 μM). Its peak excitation shifts from 340 nm to 380 nm when Ca^{2+} binds. The emission peak can be detected at 510 nm. This principle enables an interpretation; that is, the increase of cytosolic Ca^{2+} results in signal amplification at 340 nm. In the meantime, the fluorescence decrease was observed during excitation at 380 nm. Prior to imaging, cells were incubated with storage buffer containing Fura-2/AM (3.3 μM) in the dark for 45 minutes at room temperature. Afterwards, Fura-2/AM was removed, and cells were washed with storage buffer three times. Cells were maintained in the storage buffer until imaging (110).

2.6.2 Mitochondrial Ca^{2+} measurements

Mitochondria-targeted 4mtD3cpv cameleon is a FRET-based ratiometric Ca^{2+} sensor (107). The construct contains CaM (a Ca^{2+} binding domain) and myosin light chain kinase (M13) (an interacting domain). Both are fused in tandem between the cyan fluorescent protein (CFP) and the yellow fluorescent protein (YFP), a FRET donor and FRET acceptor respectively. A tandem duplicated cytochrome *c* oxidase subunit VIII (a signal sequence) is linked to 4mtD3cpv cameleon for targeting it to the mitochondrial inner membrane. Ca^{2+}

binding to CaM results in the conformational change, thereby bringing both fluorophores in close vicinity and subsequently triggering energy transfer from CFP to YFP (107).

2.7 Visualization of NO• dynamics

To avoid unspecific and indirect NO• measurement, C-geNOp/G-geNOp (cyan and green cytosolic probes) and mtC-geNOp/mtG-geNOp (cyan and green mitochondria-targeted probes) were used to monitor NO• signals on the level of individual cells. The construct is developed by Eroglu et al. by fusing bacterial GAF domain with respective fluorescent proteins (104). When GAF is occupied, the florescence of fluorophore is quenched due to GAF-NO• interaction (104).

As the G-geNOp was basically used in the present study, cells expressing G-geNOp were excited at 480 nm, and the fluorescence signals were collected at 515 nm. The probe is reversible in binding NO• and the fluorescence declines immediately after NO• release from GAF domain. Prior to imaging, cells were incubated with iron buffer for 20 minutes and then were washed twice with HEPES buffer (104).

2.8 Mitochondrial membrane potential ($\Delta\Psi_{mito}$) depolarization and measurements using TMRM

TMRM (a cell-permeant, cationic, red-orange fluorescent dye) was used in monitoring $\Delta\Psi_{mito}$ depolarization during mitochondrial bioenergetic collapse (112). Prior to $\Delta\Psi_{mito}$ measurements, EA.hy926 cells were loaded with EH-buffer containing TMRM dye (100 nM) for 10 minutes at room temperature. Then, extracellular dye was washed out three times with storage buffer, and cells were incubated in the same buffer for experiments. To dissipate $\Delta\Psi_{mito}$, cells were treated with HEPES buffer containing Ca^{2+} or EGTA in the presence of OXPHOS inhibitors, including antimycin (5 μM) and oligomycin (1 μM) (5, 101).

2.9 Fluorescence microscopes

An advanced wide-field fluorescence microscope Till iMIC equipped with a motorized sample stage, a polychrome V (Till Photonics, Graefelfing, Germany), a 40× objective lens (alpha Plan Fluar 40x, Zeiss, Göttingen, Germany), the filter sets with dichromatic mirrors (Till Photonics, Graefelfing, Germany) and a charge-coupled device camera (AVT Stingray

F145B, Allied Vision Technologies, Stadtroda, Germany) was used in imaging $NO^{\bullet}$, Ca^{2+} and TMRM.

Confocal visualizations of mtC-geNOp/mtG-geNOp in HeLaS3 cells, G-geNOp in EA.hy926 cells and eNOS-RFP in HEK293 cells were performed by using a confocal spinning disk microscope (Axio Observer.Z1, Zeiss, Göttingen, Germany). The microscope is equipped with a 40× objective lens (Plan-Neofluar 40×/1.3 oil, Zeiss, Göttingen, Germany), a 100× objective lens (Plan-Fluar 100×/1.45 oil, Zeiss, Göttingen, Germany), AOTF-based laser merge module for laser line 405, 445, 473, 488, 551 and 561 nm (Visitron Systems), a motorized filter wheel on the emission side and a Nipkow-based confocal scanning unit (CSU-X1, Yokogawa Electric Corporation, Tokyo, Japan). The fluorescent images were captured with a charged CCD camera (CoolSNAP-HQ, Photometrics, Tucson, AZ, USA). The VisiView (Universal Imaging, Visitron Systems) acquisition software was used in acquiring recorded fluorescent data (110).

During the experiments, all working buffers were applied to the cells using a gravity-based perfusion system connected with a conventional vacuum pump (Chemistry diaphragm pump ME 1C, Vacuubrand, Wertheim, Germany).

2.10 Imaging system configurations, data acquisitions and analyses

2.10.1 Single-cell cytosolic Ca^{2+} imaging

Till iMIC with wide field imaging system was the main microscope. Cells were visualized using 40x oil-immersion objective under continuous perfusion of either Ca^{2+}-free HEPES buffer or EGTA buffer with ATP (100 μM). For Ca^{2+} measurements, Fura-2/AM-loaded cells were alternatively excited at 340 and 380 nm. Fura-2 fluorescence emission was collected at 510 nm. Fluorescent images were recorded with a CCD camera (AVT Stingray F145B). Data acquisitions were carried out by The Live Acquisition 2.0.0.12 Software (Till Photonics). Ca^{2+} experimental results were expressed as the ratio of F_{340}/F_{380}. Background fluorescent values are obtained from region-of-interest (ROI) in each imaging drawn in a cell-free area. The formula used in calculation is shown below.

$$\text{Ratio}\left(\frac{F_{340}}{F_{380}}\right) = \frac{F_{340\ \text{Cell}} - F_{340\ \text{Background}}}{F_{380\ \text{Cell}} - F_{380\ \text{Background}}}$$

Simultaneous measurements of both Ca^{2+} and $NO^{\bullet}$ were accomplished on Till iMIC with an ultrafast switching monochromator (polychrome V). Imaging system is described in 2.10.3.

2.10.2 Single-cell mitochondrial Ca^{2+} imaging

The wavelength at 430 nm was set to excite the 4mtD3cpv cameleon. The emitted fluorescence was collected using the dichrotome dual emission filter set (dichroic 535dcxr, CFP emitter 480/18 nm and YFP emitter 535/3 nm). The fluorescent images were captured with CCD camera (AVT Stingray F145B). Data are acquired using The Live Acquisition 2.0.0.12 software (Till Photonics). The acquired FRET results were then analyzed and shown as the ratio of F_{535}/F_{480}.

2.10.3 Single-cell cytosolic $NO^{\bullet}$ imaging

For $NO^{\bullet}$ visualizations, C-geNOp/mtC-geNOp and G-geNOp/mtG-geNOp were excited at 430 nm (CFP) and 480 nm (GFP), and the emitted fluorescence was recorded at 480 nm (CFP) and 515 nm (GFP), respectively. The Live Acquisition 2.0.0.12 software (Till Photonics) was employed for the acquisition of experimental data. Fluorescence photobleaching was corrected by calculating the bleaching function F_0 for an individual cell using a one phase exponential decay equation for curve fitting. The acquired data were expressed as $1\text{-}F/F_0$ or $\Delta F_{Intensity}$ (%) where F is a background-subtracted fluorescent value.

2.10.4 TMRM measurements

Upon mitochondrial bioenergetic collapse, the changes in $\Delta\Psi_{mito}$ were monitored and TMRM was visualized at an excitation of 550 nm and emission of 575 nm. At the beginning of the recording, the reticular mitochondria are bright red-orange. The color becomes dimmed after cells were exposed to antimycin and oligomycin for 7 minutes. This phenomenon is the indicative of mitochondrial depolarization (more positive $\Delta\Psi_{mito}$) caused by perturbed bioenergetics and loss of H^+ gradient. Bleaching function F_0 for fluorescent dye bleaching correction was used for individual curve fitting. The acquired data were expressed as F/F_0 where F is a background-subtracted fluorescent value.

2.11 Western blot analysis of eNOS and phospho-eNOS protein expressions

siRNA-transfected EA.hy926 cells were incubated either with vehicle or ATP (100 μM) at 37 °C for 3 or 5 minutes. Then, cells were harvested and homogenized in ice-cold RIPA lysis buffer containing EDTA (2 mM), protease and phosphatase inhibitors. Protein concentration was determined with PierceTM BCA Protein Assay Kit using bovine serum albumin as standard. Western blot was performed to determine expression level of eNOS and its phosphorylated form. Denatured protein samples (30 μg) were loaded onto 10% polyacrylamide gel containing 0.1% sodium dodecyl sulfate and electrophoretically separated. Separated proteins were then transferred onto nitrocellulose membranes. Prior to antibody incubation, the non-specific binding sites on the membrane were blocked with 5% skimmed milk in Tris-buffered saline containing 0.1% tween-20 for 1 hour. The membranes were incubated with a primary antibody against eNOS (1:2000), phospho-eNOS (pSer1177) (1:1000), or β-actin (1:200,000) overnight at 4 °C. Thereafter, membranes were washed 3 times and incubated for 1 hour with a horseradish peroxidase-conjugated anti-mouse IgG secondary antibody (1:5000). eNOS and its phosphorylated protein bands were visualized using enhanced chemiluminescence (ECL) technique. Density of protein bands was quantified using the Fusion SL system.

2.12 Statistical analyses

The acquired data were analyzed using the GraphPad Prism software version 5.04 for Window (GraphPad Software, San Diego, CA, USA). Data are presented as mean ± standard error of mean (SEM) of independent experiments (N). For comparisons between two groups, two-tailed student t-test was used for evaluation of statistical significance. A p value between 0.01 and 0.05 was considered significant and indicated with "*", a p value between 0.001 and 0.01 with "**" (very significant) and a p value less than 0.001 with "***" (highly significant). For multiple-group comparisons, one-way ANOVA with Barlett's test for equal variances and Tukey's Multiple Comparison test were used for evaluating statistical significance expressed as described above. Represented data as appeared as bars and line graphs and western blot images were either average or representative curves of independent experiments.

CHAPTER 3

RESULTS

3.1 Real-time monitoring of NO• dynamics in human endothelial cell surrogate (EA.hy926 cells)

The G-geNOp, the novel protein-based fluorescent NO• probe, was utilized in real-time investigation of NO• dynamics in single EA.hy926 cells. Binding of NO• in the vicinity of EGFP in G-geNOp induced a fluorescence quenching; yet, in the absence of cytosolic NO•, the probe became unoccupied and the EGFP fluorescence was back to unquenched state, demonstrating a reversible interaction between the probe and the free NO• (Figure 3.1A). Figure 3.1B represents a high resolution confocal image of G-geNOp-expressing EA.hy926 cells. The cells showed a bright green fluorescence in both cytosol and nucleus. According to the sources of Ca^{2+} that can contribute to the eNOS activation and cytosolic NO•, the experimental protocols (cell treatments) were designed to dissect the endothelial NO• production with regard to different Ca^{2+} sources. First, we mobilized endoplasmic reticulum Ca^{2+} using ATP (IP_3-generating agonist) simultaneously with intracellular Ca^{2+} calibration using EGTA, which chelated extracellular free Ca^{2+} with high affinity. Following complete endoplasmic reticulum Ca^{2+} depletion, the cells were then perfused with Ca^{2+}-containing HEPES buffer in the presence of ATP to ensure that the increase of NO• was dependent on extracellular Ca^{2+} entering the cells during store-operated Ca^{2+} entry (SOCE). To elucidate NO• production, G-geNOp-expressing EA.hy926 cells were first stimulated with HEPES buffer containing ATP and EGTA. The result showed that the ATP evoked an initiation of transient NO• signals, and the signals declined after the amplitudes were reached at minute 4.50 (Figure 3.1C). Cytosolic NO• levels rapidly recovered upon subsequent addition of Ca^{2+}/ATP-containing HEPES buffer to ATP-stimulated cells, and they remained elevated in the presence of ATP (amplitude at minute 12.00) (Figure 3.1C). However, within a few minutes, the signals gradually decreased back to basal level upon ATP washout (Figure 3.1C). This present result demonstrates the importance of SOCE for sustained eNOS activation and continuous NO• synthesis. Furthermore, as shown in Figure 3.1D, the simultaneous measurements of cytosolic Ca^{2+} and NO• confirmed that both intracellular and extracellular

Ca^{2+} signals were fundamental for eNOS activation. Therefore, the endothelial $NO^{\bullet}$ production in this cell type is primarily controlled by cytosolic Ca^{2+}.

Another two experimental sets were performed to test the sensitivity of geNOp when the eNOS was inhibited by L-N^{G}-nitro arginine, a potent NOS inhibitor. In control EA.hy926 cells expressing G-geNOp, the $NO^{\bullet}$ signals clearly elevated immediately after ATP-evoke cytosolic Ca^{2+} increases (Figure 3.2A). Conversely, the signals obtained from the cells pretreated with L-N^{G}-nitro arginine were abolished despite intracellular Ca^{2+} increases (Figure 3.2B). The maximum average signals are represented in Figure 3.2C, $p < 0.001$ vs. control. Moreover, a further confirmation of sensor specificity was demonstrated by using G-geNOp^{mut} (an insensitive mutated $NO^{\bullet}$ probe). EA.hy926 cells expressing G-geNOp^{mut} treated with ATP did not produce any significant fluorescence signal compared to control cells, $p < 0.001$ vs. G-geNOp (Figure 3.3). Whereas, the cells expressing G-geNOp, which is the sensitive probe, could sense increased $NO^{\bullet}$ content and produce fluorescence signals. These experimental results confirm that geNOp technology is suitable for a specific real-time imaging of endothelial $NO^{\bullet}$ dynamics on the level of individual cells.

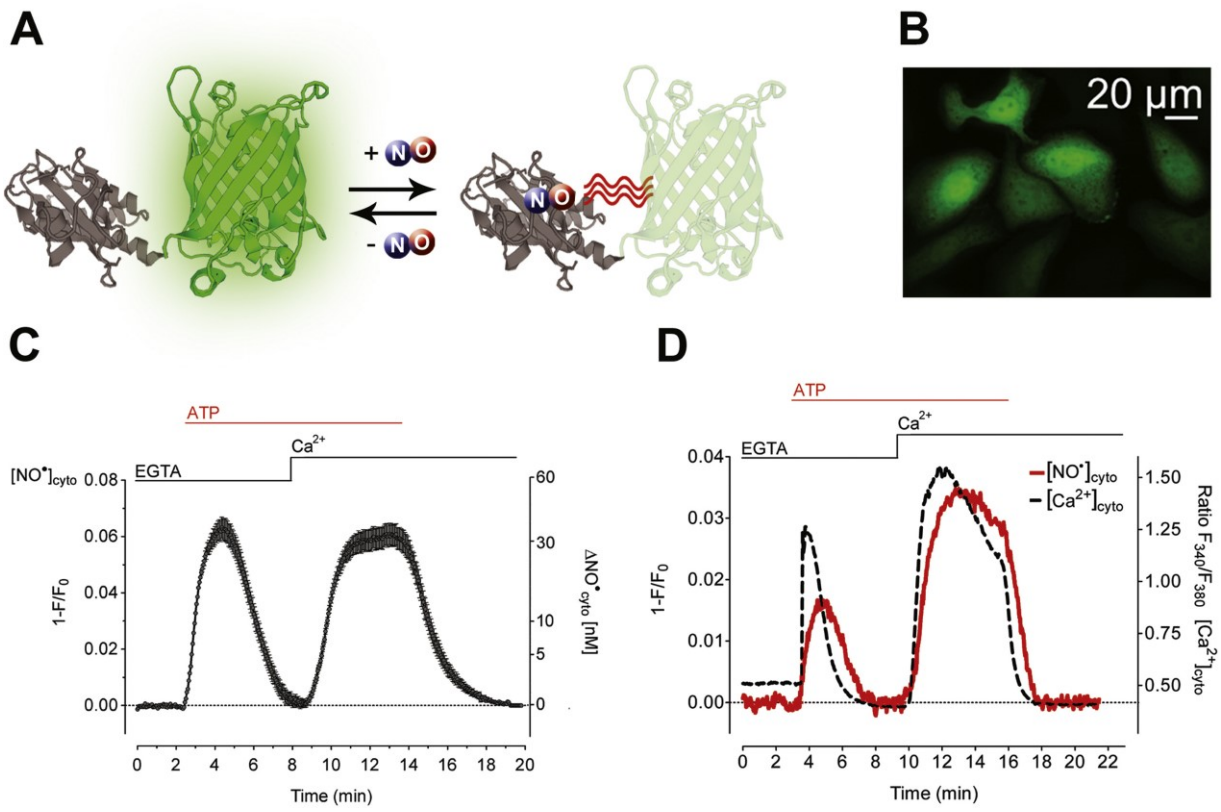

Figure 3.1 Live-cell NO• imaging in endothelial cells. (A) Schematic illustration of G-geNOp consisting of the enhanced green fluorescent protein (EGFP) fused to the bacteria-derived NO•-binding domain (GAF). (B) Representative image of EA.hy926 cells expressing G-geNOp. (C) Average curve representing NO• signal ($[NO^{\bullet}]_{cyto}$) obtained from EA.hy926 cells perfused with ATP (100 μM) in the absence and presence of extracellular Ca^{2+} (2 mM) (N = 40). (D) Representative simultaneous recordings of $[NO^{\bullet}]_{cyto}$ (red line) and cytosolic Ca^{2+} signals ($[Ca^{2+}]_{cyto}$, dashed black line) over time in a single Fura-2/AM loaded EA.hy926 cell expressing G-geNOp. Cells was treated with ATP (IP_3-generating agonist) in the absence and presence of Ca^{2+}. EGTA (1 mM) was used as a Ca^{2+} chelator. Data were expressed as mean ± SEM. [Reproduced from Charoensin S, Emrah E, Opelt M, et al. Intact mitochondrial Ca^{2+} uniport is essential for agonist-induced activation of endothelial NO• synthase (eNOS). Free Radic Biol Med. 2017;102:248-59. (105), with permission of publisher Elsevier Inc. Copyright 2016.]

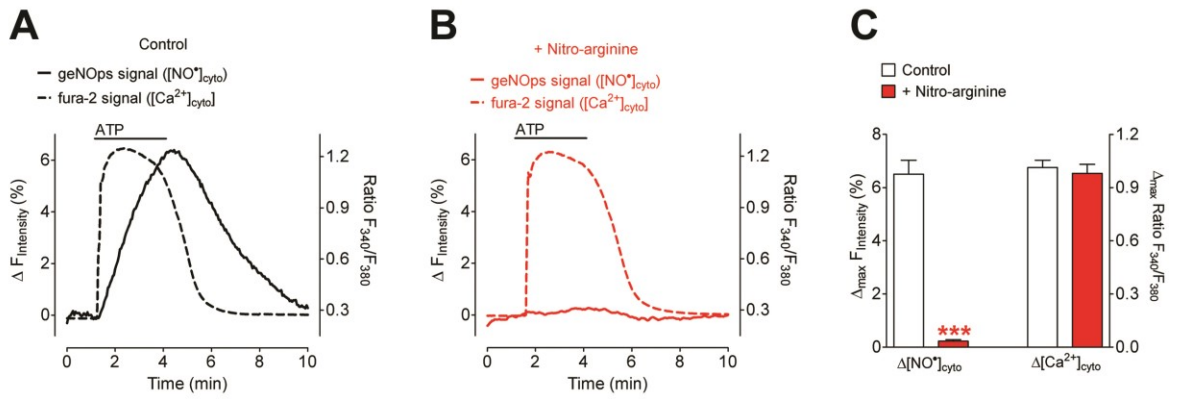

Figure 3.2 L-N^G-nitro arginine inhibits NO• production in EA.hy926 cells. (A) Representative curves showing NO• dynamics ($[NO^{\bullet}]_{cyto}$, solid black line) and Fura-2 signal ($[Ca^{2+}]_{cyto}$, dashed black line) in response to ATP (100 μM) obtained from G-geNOp expressing EA.hy926 cells loaded with Fura-2/AM. (B) Representative curves of $[NO^{\bullet}]_{cyto}$ (solid red line) and $[Ca^{2+}]_{cyto}$ (dashed red line) obtained from EA.hy926 cells pre-incubated with L-N^G-nitro arginine (1 mM) for 10 minutes prior to ATP treatment. (C) Bars show maximal average $[NO^{\bullet}]_{cyto}$ and $[Ca^{2+}]_{cyto}$ from control cells (N = 6) and L-N^G-nitro arginine-pretreated cells (N = 6) in response to ATP. In respective experiments, L-N^G-nitro arginine was used as an eNOS inhibitor. Data were obtained from independent experiments and expressed as mean ± SEM. *p* value less than 0.001 (***). [Reproduced from Charoensin S, Emrah E, Opelt M, et al. Intact mitochondrial Ca^{2+} uniport is essential for agonist-induced activation of endothelial NO• synthase (eNOS). Free Radic Biol Med. 2017;102:248-59. (105), with permission of publisher Elsevier Inc. Copyright 2016.]

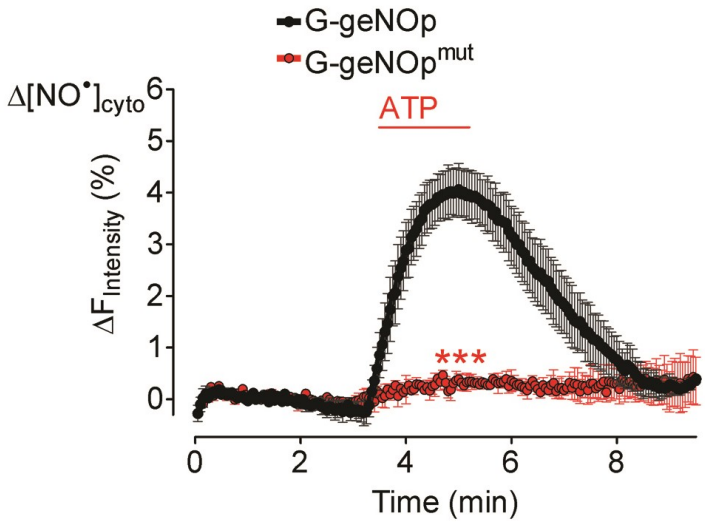

Figure 3.3 G-geNOp^{mut}-expressing EA.hy926 cells show steady NO• signal in response to ATP stimulation of intracellular Ca^{2+} release. Curves represent mean fluorescence signals obtained from EA.hy926 cells expressing either the NO•-sensitive G-geNOp or the NO•-insensitive G-geNOp^{mut}. Data were gathered from independent experiments (N = 9 for G-geNOp and N = 9 for G-geNOp^{mut}) and expressed as mean ± SEM. *p* value less than 0.001 (***). [Reproduced from Charoensin S, Emrah E, Opelt M, et al. Intact mitochondrial Ca^{2+} uniport is essential for agonist-induced activation of endothelial NO• synthase (eNOS). Free Radic Biol Med. 2017;102:248-59. (105), with permission of publisher Elsevier Inc. Copyright 2016.]

Apart from $NO^{\bullet}$ imaging in cytosol, the present study also sought to investigate its dynamics within endothelial mitochondria. To archive this purpose, two mitochondria-targeted $NO^{\bullet}$ probes, including mtG-geNOp and mtC-geNOp, were transiently expressed in EA.hy926 cells. The confocal imaging represents a co-localization of vibrant mtC-geNOp and MitoTracker™ Red CMXRos (Figure 3.4, upper panel). Likewise, EA.hy926 cells expressing mtG-geNOp showed preferential localization with the mitochondrial marker (Figure 3.4, lower panel). As endothelial mitochondria are where $NO^{\bullet}$ can penetrate, accumulate and take effects, the experiments were then set out to investigate its dynamics within the organelle during ATP activation of purinergic signaling and subsequent Ca^{2+} release and entry. Upon Ca^{2+}-triggered eNOS activation, mtG-geNOp and G-geNOp could sense the transient rises of $NO^{\bullet}$ within mitochondria and cytoplasm, respectively (Figure 3.5A and 3.5B). In the continuous recordings, both cytosolic and mitochondrial probes very well detected $NO^{\bullet}$ which was liberated from a donor NOC-7 (Figure 3.5A and 3.5B). Conversely, cells expressing mutant probe mtG-geNOp^{mut} could barely detect the signal (Figure 3.5A, lower curve). Comparing $NO^{\bullet}$ signals in basal and stimulated condition, it was found that the cells produced relatively low amount of it at resting cytosolic Ca^{2+}, while they generated significantly high amount upon ATP-evoked cytosolic Ca^{2+} rise, $p < 0.05$ vs. basal (Figure 3.5C). To perform simultaneous measurements of $NO^{\bullet}$ signals in both mitochondria and cytosol, mtC-geNOp and G-geNOp were transiently expressed in EA.hy926 cells. Both probes localized very well in their targeting areas (Figure 3.5D). Moreover, the simultaneous recordings of mtC-geNOp and G-geNOp signals precisely revealed the concurrent $NO^{\bullet}$ dynamics between these two cell compartments (Figure 3.5E). Similarly, as represented in Figure 3.6, the cells co-expressing mtG-geNOp and C-geNOp exhibited the comparable $NO^{\bullet}$ dynamics as observed in the previous measurements shown in Figure 3.5E. Consequently, based on the present results, the geNOp firmly demonstrates its reliability and sensitivity in real-time investigation of $NO^{\bullet}$ dynamics within specific cell compartments.

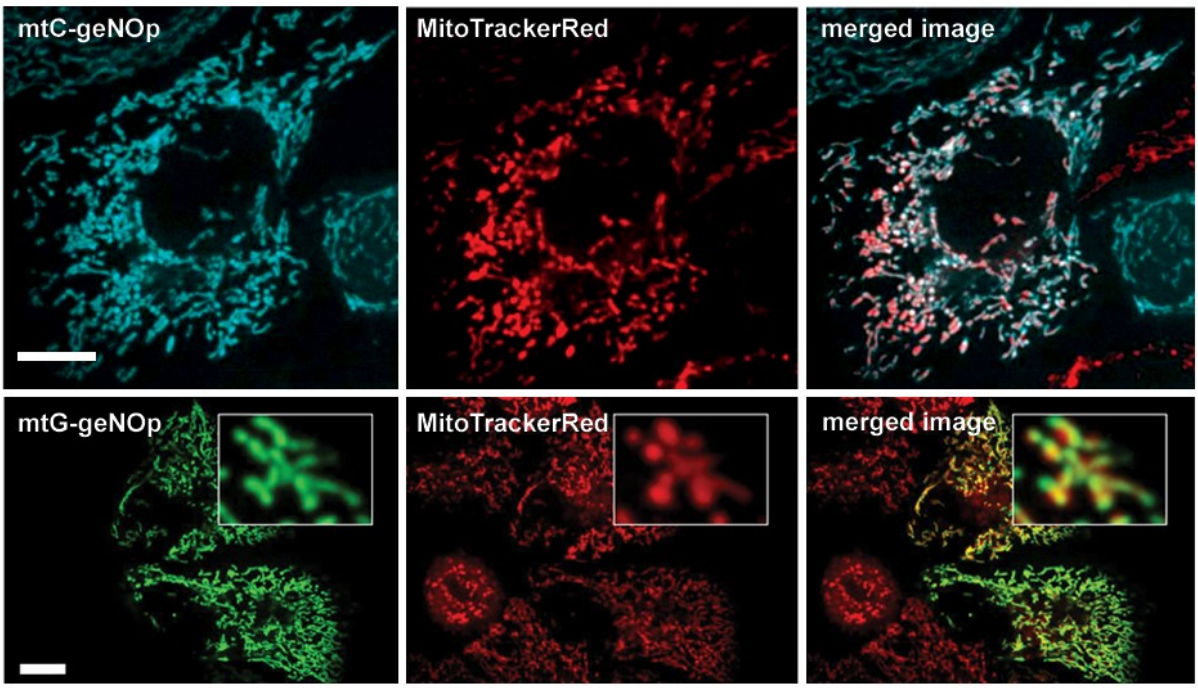

Figure 3.4 Confocal imaging representing co-localizations of mtC-geNOp or mtG-geNOp and MitoTracker™ Red CMXRos in HeLaS3 cells. HeLaS3 cells were transiently transfected with either mtC-geNOp or mtG-geNOp. Prior to confocal visualization, the transfected cells were pre-incubated with MitoTracker™ Red CMXRos. [Reproduced from Eroglu E, Gottschalk B, Charoensin S, et al. Development of novel FP-based probes for live-cell imaging of nitric oxide dynamics. Nat Commun. 2016;7:10623. (104), with permission of publisher Nature Publishing Group. Copyright 2016.]

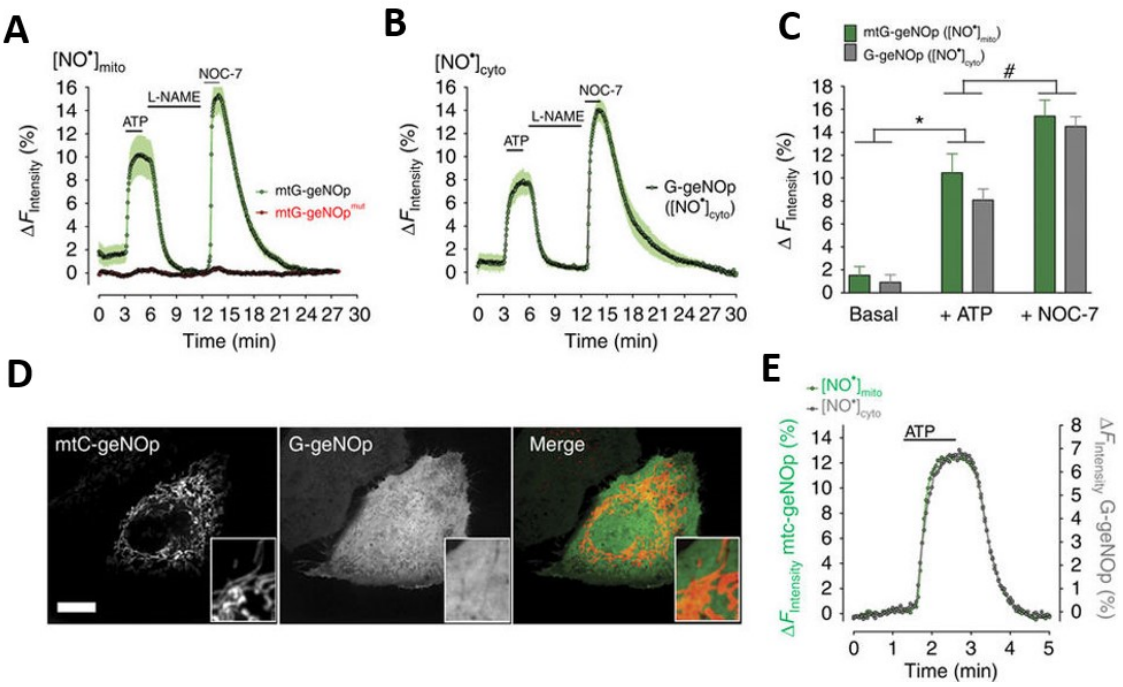

Figure 3.5 Mitochondrial NO• imaging in EA.hy926 cells. (A) Line curves showing average mitochondrial NO• signals ($[NO^{\bullet}]_{mito}$) in EA.hy926 cells expressing mtG-geNOp or its mutant version (mtG-geNOp^{mut}) in response to ATP (100 μM) and NOC-7 (10 μM). (B) Average G-geNOp signal of intracellular NO• in EA.hy926 cells treated with ATP and NOC-7. (C) Columns showing average maximal amplitudes of mtG-geNOp signal (3.5A) and G-geNOp signal (3.5B) under the same treatments. (D) Confocal images representing mtC-geNOp and G-geNOp expression in EA.hy926 cells, scale bar = 10 μm. (E) Representative mtC-geNOp and G-geNOp signals obtained from simultaneous measurements in ATP-treated EA.hy926 cell. L-NAME (1 mM) and NOC-7 were used as a NOS inhibitor and NO• donor, respectively. Unpaired t-test was used to analyze significant difference between basal condition and treatment with ATP or NOC-7, * $p < 0.05$ vs. basal and # $p < 0.05$ vs. +ATP. [Reproduced from Eroglu E, Gottschalk B, Charoensin S, et al. Development of novel FP-based probes for live-cell imaging of nitric oxide dynamics. Nat Commun. 2016;7:10623. (104), with permission of publisher Nature Publishing Group. Copyright 2016.]

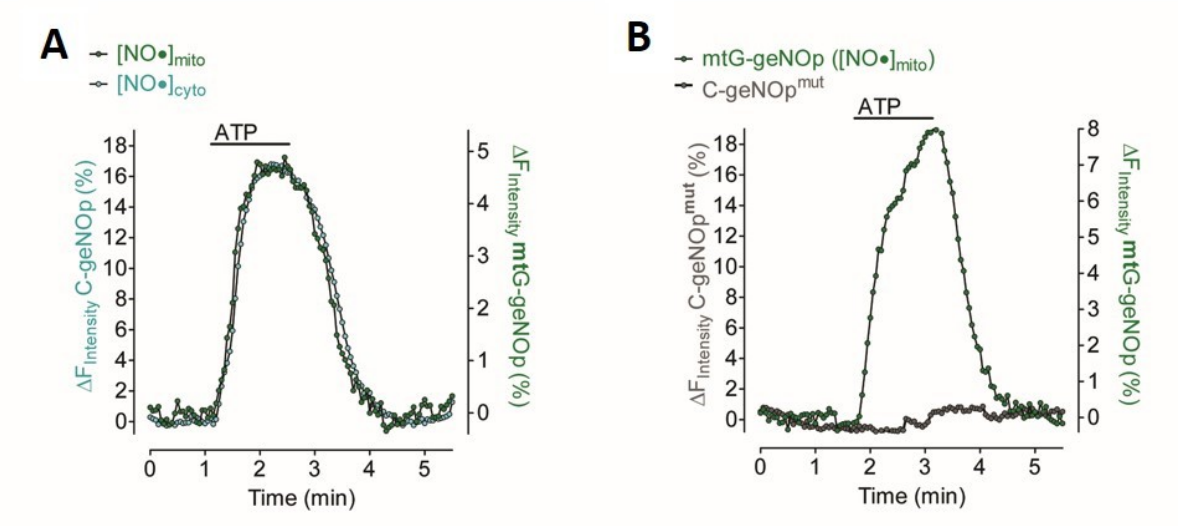

Figure 3.6 Simultaneous measurements of mitochondrial and cytosolic NO˙ signals. (A) Representative C-geNOp signal vs. mtG-geNOp signal obtained from EA.hy926 cells in response to ATP (100 μM) stimulation of endoplasmic reticulum Ca^{2+} release. (B) Representative mtG-geNOp signal vs. mutant C-geNOp signal in response to ATP. [Reproduced from Eroglu E, Gottschalk B, Charoensin S, et al. Development of novel FP-based probes for live-cell imaging of nitric oxide dynamics. Nat Commun. 2016;7:10623. (104), with permission of publisher Nature Publishing Group. Copyright 2016.]

3.2 Genetic manipulation of mitochondrial Ca^{2+} uptake machinery on $NO^{\bullet}$ production in EA.hy926 cell line and primary human umbilical vein endothelial cells (HUVECs)

3.2.1 EMRE and MCU silencing reduces ATP-induced mitochondrial Ca^{2+} uptake and $NO^{\bullet}$ production in EA.hy926 cells

EA.hy926 cells were transfected with siRNAs against EMRE and MCU, two key components of the MCU complex, to investigate whether mitochondrial Ca^{2+} uptake modulated endothelial $NO^{\bullet}$ production. The perturbation of MCU complex substantially diminished mitochondrial Ca^{2+} signals in response to endoplasmic reticulum Ca^{2+} release and entry. However, the basal mitochondrial Ca^{2+} contents were only slightly dropped (Figure 3.7A). Statistical analyses showed that average basal levels of mitochondrial Ca^{2+} accumulation were indifferent between control and EMRE/MCU-treated cells ($p = 0.0518$) in Ca^{2+}-free HEPES buffer (EGTA buffer) (Figure 3.7A, left columns). However, knock-down of both genes resulted in a significant decrease of average maximum mitochondrial Ca^{2+} signals when cells were treated with EGTA buffer in the presence of ATP ($p = 0.0029$) and ATP-containing HEPES buffer ($p = 0.0169$) (Figure 3.7A, left and right columns). Under the same experimental conditions, intracellular Ca^{2+} transients were only decreased at the plateau phase during store operated Ca^{2+} entry (Figure 3.7B). This molecular event confirms that the mitochondrial Ca^{2+} uptake facilitates SOCE in endothelial cells. Statistical analyses indicated that there was no significant change in cytosolic Ca^{2+} contents in basal state, ATP-stimulated endoplasmic reticulum Ca^{2+} release and maximum Ca^{2+} entry (Figure 3.7B, columns). Interestingly, siEMRE/siMCU-ablated cells considerably exhibited the decreased $NO^{\bullet}$ signals upon IP_3-dependent Ca^{2+} mobilization from the intracellular store (Figure 3.7C). The average $NO^{\bullet}$ signal of the cells ablated from EMRE and MCU was considerably dropped to 60% when compared to the average percentage of control cells ($p = 0.0068$ (Ca^{2+} release phase) and $p = 0.0042$ (Ca^{2+} entering phase), Figure 3.7C, left and middle columns). G-geNOp^{mut}-expressing cells (control cells regarding probe sensitivity) transiently transfected with either scrambled siRNA or siEMRE/siMCU did not show any significant changes of the average fluorescence signals in response to ATP (Figure 3.7C, right columns). The investigation of endothelial $NO^{\bullet}$ dynamics in EA.hy926 cells stimulated with low concentrations of ATP was also carried out. Similar to those results observed in cells treated with supra-physiological ATP, cells with EMRE and MCU knock-down markedly produced much less $NO^{\bullet}$ when stimulated with

various doses of ATP ranging from 1-100 μM (Figure 3.7D). The average $NO^{\bullet}$ signals of EMRE/MCU-silenced cells treated with 1 μM ATP (p = 0.0045), 5 μM ATP (p = 0.0087), or 100 μM ATP (p = 0.0012) were statistically different to respective control cells (Figure 3.7D, columns). These results indicate that the MCU complex-mediated mitochondrial Ca^{2+} uptake is closely associated with endothelial NOS activation, regardless of agonist concentration-dependent purinergic activation of intracellular Ca^{2+} mobilization.

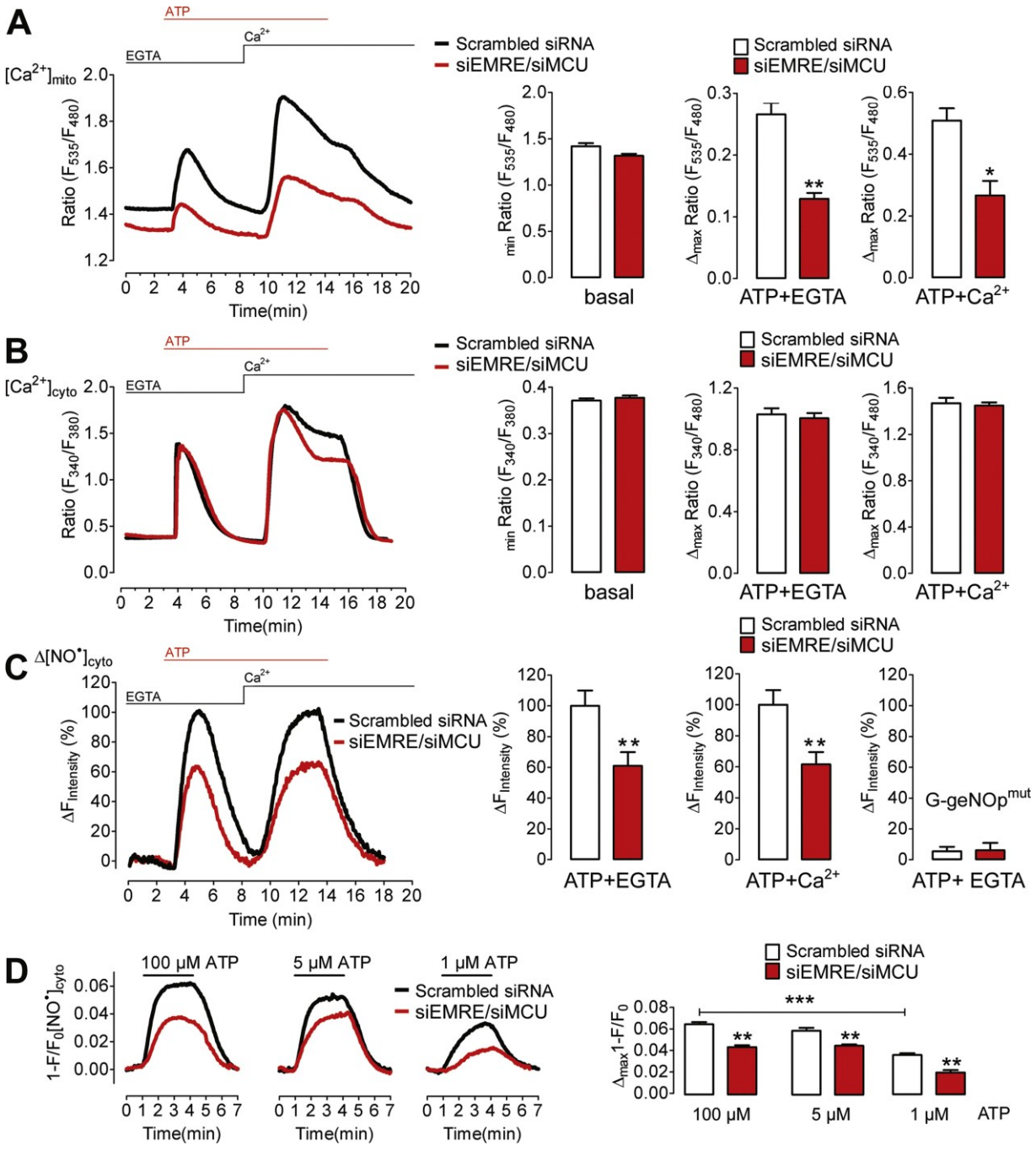

Figure 3.7 EMRE and MCU silencing reduces NO• production in EA.hy926 cells in response to ATP-evoked Ca^{2+} release. (A) Average curves of $[Ca^{2+}]_{mito}$ in either control (black, N = 3) or EMRE/MCU-knocked down (red, N = 3) EA.hy926 cells upon stimulation with ATP (100 μM) in the absence and presence of extracellular Ca^{2+} (2 mM). Left columns show average basal $[Ca^{2+}]_{mito}$ ($_{min}$ Ratio (F_{535}/F_{480})). Middle and right columns show average maximal $[Ca^{2+}]_{mito}$ (Δ_{max} Ratio (F_{535}/F_{480})) in response to ATP+EGTA and ATP+Ca^{2+}. (B)

Curves representing averages of $[Ca^{2+}]_{cyto}$ between control (N=6) and EMRE/MCU-silenced (N = 7) EA.hy926 cells stimulated with ATP. Bars represent the comparisons between basal $[Ca^{2+}]_{cyto}$ ($_{min}$ Ratio (F_{340}/F_{380})) and the respective maximal $[Ca^{2+}]_{cyto}$ (Δ_{max} Ratio (F_{340}/F_{380})) under the same conditions and treatment. (C) Representative curves of cytosolic $NO^{\bullet}$ ($\Delta[NO^{\bullet}]_{cyto}$) in response to ATP stimulation, with or without extracellular Ca^{2+}. Maximal fluorescence signals (amplitudes) of scrambled siRNA- or siMCU/siEMRE-treated cells (N = 17 each) are defined as 100%. Left and middle columns show average $\Delta[NO^{\bullet}]_{cyto}$ under the respective conditions and treatment. Right columns represent amplitudes of $NO^{\bullet}$-insensitive G-geNOp^{mut} in the presence of ATP in HEPES buffer containing EGTA (1 mM), control cells (N = 11) and siEMRE/siMCU-treated cells (N = 10). (D) Average curves of Ca^{2+}-triggered $NO^{\bullet}$ formation in response to ATP (1 μM, 5 μM and 100 μM) in control cells (N = 3) and siEMRE/siMCU-transfected EA.hy926 cells (N = 3). Columns represent maximal $[NO^{\bullet}]_{cyto}$ in response to different ATP concentrations. "*" for p value < 0.05, "**" for p value < 0.01 and "***" for p value less than 0.001. [Reproduced from Charoensin S, Emrah E, Opelt M, et al. Intact mitochondrial Ca^{2+} uniport is essential for agonist-induced activation of endothelial $NO^{\bullet}$ synthase (eNOS). Free Radic Biol Med. 2017;102:248-59. (105), with permission of publisher Elsevier Inc. Copyright 2016.]

3.2.2 EMRE and MCU knock-down results in NO• decreases in HUVECs

As shown in the previous part, silencing of both EMRE and MCU in EA.hy926 cells resulted in a reduction of NO• transients. The next question that arose after was that how this silencing modulated NO• dynamics in primary endothelial cells. To figure it out, we first performed live-cell imaging to compare both Ca^{2+} and NO• dynamics in primary human umbilical vein endothelial cells (HUVECs) and EA.hy926 cells. The results showed that HUVECs from pooled donors could produce less maximal cytosolic Ca^{2+} transients in response to ATP compared to EA.hy926 cells (p = 0.0050) (Figure 3.8A, right columns), whereas the basal Ca^{2+} signals were identical in both cell types (Figure 3.8A, left columns). The maximal mitochondrial Ca^{2+} signals in HUVECs were found to be higher than in endothelial cell surrogate (Figure 3.8B). Respective NO• imaging demonstrated that the average NO• content of HUVECs was substantially lower than the content of EA.hy926 cells (p = 0.0366) (Figure 3.8C, left columns). Notably, considering the slopes, HUVECs showed rather slow NO• kinetics, while EA.hy926 cells were much faster (Figure 3.8C, curves and right columns). These results indicate a difference in the rates of eNOS coupling reaction which is activated by cytosolic Ca^{2+} elevations in both cell types.

Further experiments regarding perturbation of MCU complex revealed the negative effect of it on mitochondrial Ca^{2+} uptake and NO• generations in HUVECs. The EMRE and MCU silencing considerably reduced mitochondrial Ca^{2+} accumulation in HUVECs treated with ATP compared to scrambled siRNA-treated cells (p = 0.0032) (Figure 3.8D, right columns). Compared with the respective control cells, the siEMRE/siMCU-treated cells were able to generate significantly less amount of NO• (p = 0.0193) with considerably slower kinetics (p = 0.0206) (Figure 3.8E, left and right columns). The diminished NO• level occurred with the reduced mitochondrial Ca^{2+} uptake capacity. Based on the observed results, during ATP-triggered intracellular Ca^{2+} release and entry, the intact MCU complex and the mitochondrial Ca^{2+} signals are crucial for eNOS-derived NO• synthesis in both primary HUVECs and endothelial cell surrogate.

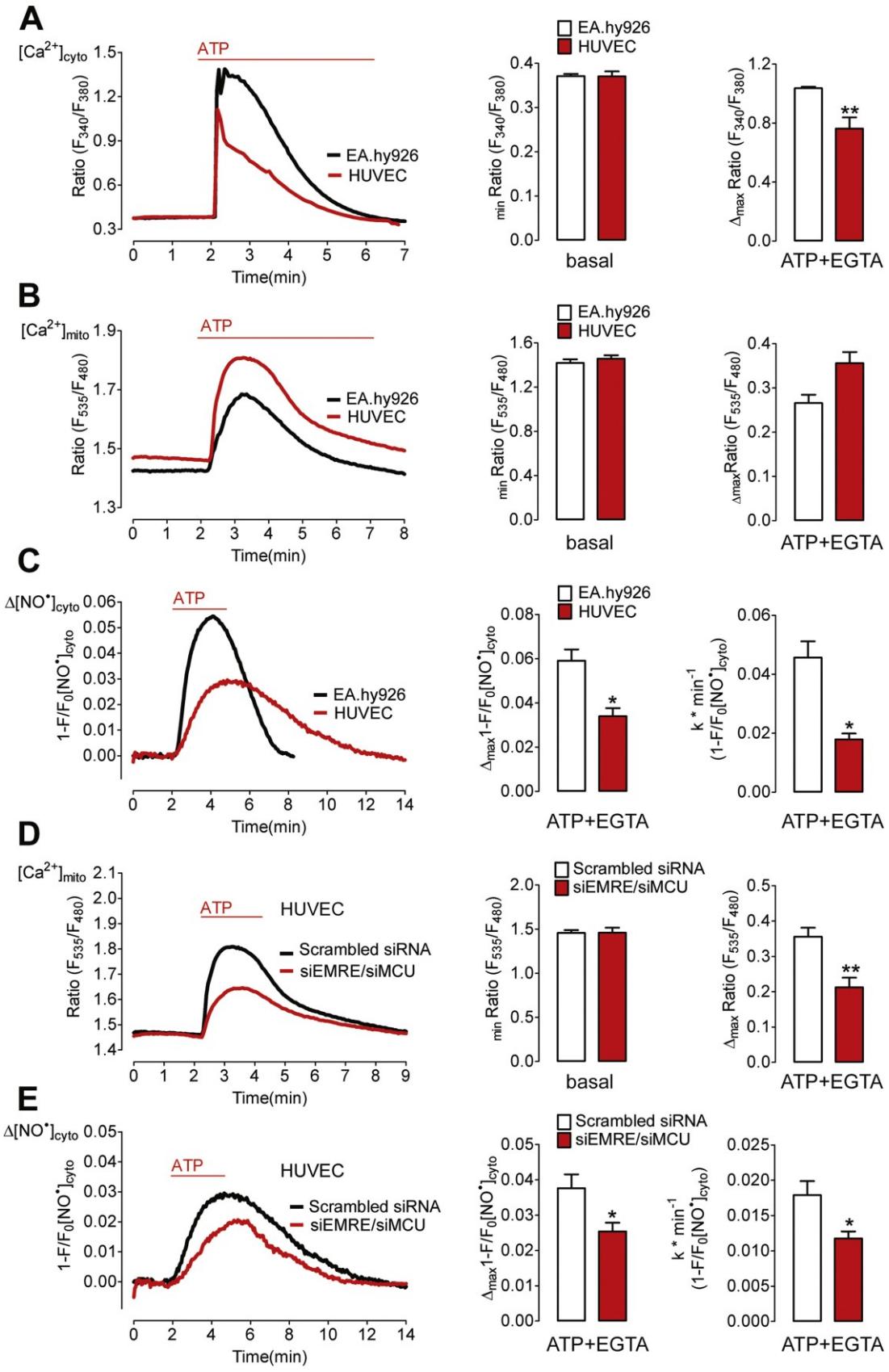
A
[Ca2+]cyto
ATP
Ratio (F340/F380)
EA.hy926
HUVEC
Time(min)
EA.hy926
HUVEC
min Ratio (F340/F380)
basal
Δmax Ratio (F340/F380)
**
ATP+EGTA
B
[Ca2+]mito
ATP
Ratio (F535/F480)
EA.hy926
HUVEC
Time(min)
EA.hy926
HUVEC
min Ratio (F535/F480)
basal
Δmax Ratio (F535/F480)
ATP+EGTA
C
Δ[NO•]cyto
ATP
1-F/F0[NO•]cyto
EA.hy926
HUVEC
Time(min)
EA.hy926
HUVEC
Δmax 1-F/F0[NO•]cyto
*
ATP+EGTA
k * min-1
(1-F/F0[NO•]cyto)
*
ATP+EGTA
D
[Ca2+]mito
ATP
HUVEC
Ratio (F535/F480)
Scrambled siRNA
siEMRE/siMCU
Time(min)
Scrambled siRNA
siEMRE/siMCU
min Ratio (F535/F480)
basal
Δmax Ratio (F535/F480)
**
ATP+EGTA
E
Δ[NO•]cyto
ATP
HUVEC
1-F/F0[NO•]cyto
Scrambled siRNA
siEMRE/siMCU
Time(min)
Scrambled siRNA
siEMRE/siMCU
Δmax 1-F/F0[NO•]cyto
*
ATP+EGTA
k * min-1
(1-F/F0[NO•]cyto)
*
ATP+EGTA

Figure 3.8 EMRE and MCU ablation diminishes NO• synthesis in HUVECs. (A) 100 μM ATP-triggered cytosolic Ca^{2+} transients expressed as Fura-2 ratio (F_{340}/F_{380}) in EA.hy926 cells (N = 6) and HUVECs (N = 6). Left bars represent average basal $[Ca^{2+}]_{cyto}$ of EA.hy926 cells and HUVECs. Right bars show average amplitudes in EA.hy926 cells and HUVECs. (B) Average mitochondrial Ca^{2+} signals obtained from EA.hy926 cells (N = 6) and HUVECs (N = 6) in response to ATP. Left bars represent ratios of basal $[Ca^{2+}]_{mito}$ of EA.hy926 cells and HUVECs. Right bars show maximal amplitudes in EA.hy926 and HUVEC cells. (C) Ca^{2+}-triggered cytosolic NO• formation ($\Delta[NO^{\bullet}]_{cyto}$) in EA.hy926 cells (N = 10) and HUVECs (N = 8). Middle bars represent maximal fluorescence changes of G-geNOp in EA.hy926 cells and HUVECs in response to ATP. Right bars show respective maximal slopes of G-geNOp fluorescence changes in EA.hy926 cells and HUVECs. (D) Average $[Ca^{2+}]_{mito}$ in HUVECs transfected with either scrambled siRNA (black curve, N = 6) or siEMRE/siMCU (red curve, N = 6) following ATP stimulation in the absence of extracellular Ca^{2+}. Middle bars represent basal $[Ca^{2+}]_{mito}$ under the same conditions and treatment. Right bars show respective maximal ratio amplitudes. (E) Average $\Delta[NO^{\bullet}]_{cyto}$ in HUVECs transfected with either scrambled siRNA (N = 8) or siEMRE/siMCU (N = 8) following ATP stimulation in the absence of extracellular Ca^{2+}. Middle bars represent maximal fluorescence changes of G-geNOp in HUVECs in response to ATP. Right bars show respective maximal slopes of G-geNOp fluorescence changes in HUVECs. "*" for p value < 0.05 and "**" for p value < 0.01. [Reproduced from Charoensin S, Emrah E, Opelt M, et al. Intact mitochondrial Ca^{2+} uniport is essential for agonist-induced activation of endothelial NO• synthase (eNOS). Free Radic Biol Med. 2017;102:248-59. (105), with permission of publisher Elsevier Inc. Copyright 2016.]

3.2.3 MICU1 ablation increases mitochondrial Ca^{2+} uptake and $NO^{\bullet}$ formation in EA.hy926 cells and primary HUVECs

Cytosolic Ca^{2+} signal has been reported to activate eNOS enzyme; nevertheless, it is not well understood whether mitochondrial Ca^{2+} promotes $NO^{\bullet}$ production (27, 97). It has been known that MICU1 acts as a gatekeeper for MCU-mediated mitochondrial Ca^{2+} uptake (43). To clarify this unclear point, MICU1 mRNA expressions in EA.hy926 cells and primary HUVECs were suppressed using siRNA. As expected, siMICU1-treated EA.hy926 cells showed significantly increased basal mitochondrial Ca^{2+} levels (p = 0.0356) compared to the cells treated with scrambled siRNA (Figure 3.9A, left columns). Furthermore, the mitochondria of treated-cells could uptake more Ca^{2+} into their matrix than mitochondria of control cells in response to ATP-evoked Ca^{2+} release in the absence and presence of extracellular Ca^{2+} (p = 0.0098, ATP+EGTA and p = 0.0151, ATP+ Ca^{2+}) (Figure 3.9A, middle and right columns). Respective cytosolic Ca^{2+} transients remained unaffected by the MICU1 knock-down (Figure 3.9B). Under the same conditions, $NO^{\bullet}$ generations in MICU1-silenced EA.hy926 cells were, however, significantly higher than in control cells (p = 0.0083, ATP+EGTA and p = 0.0079, ATP+ Ca^{2+}), 40% over the respective control cells (Figure 3.9C, left and middle columns). These results emphasize the positive modulation of mitochondria on endothelial $NO^{\bullet}$ content; that is, the increased mitochondrial Ca^{2+} uptake enhances $NO^{\bullet}$ production. Tendency of the effect of mitochondrial Ca^{2+} signals on endothelium-derived $NO^{\bullet}$ production found in HUVECs was consistent to that found in EA.hy926 cells. MICU1 silencing promoted mitochondrial Ca^{2+} accumulation in response to ATP stimulation (Figure 3.9D). Despite the increased Ca^{2+} uptake into mitochondrial matrix, the $NO^{\bullet}$ synthesis observed in MICU1-treated HUVECs was slightly increased compared to respective control cells (Figure 3.9E).

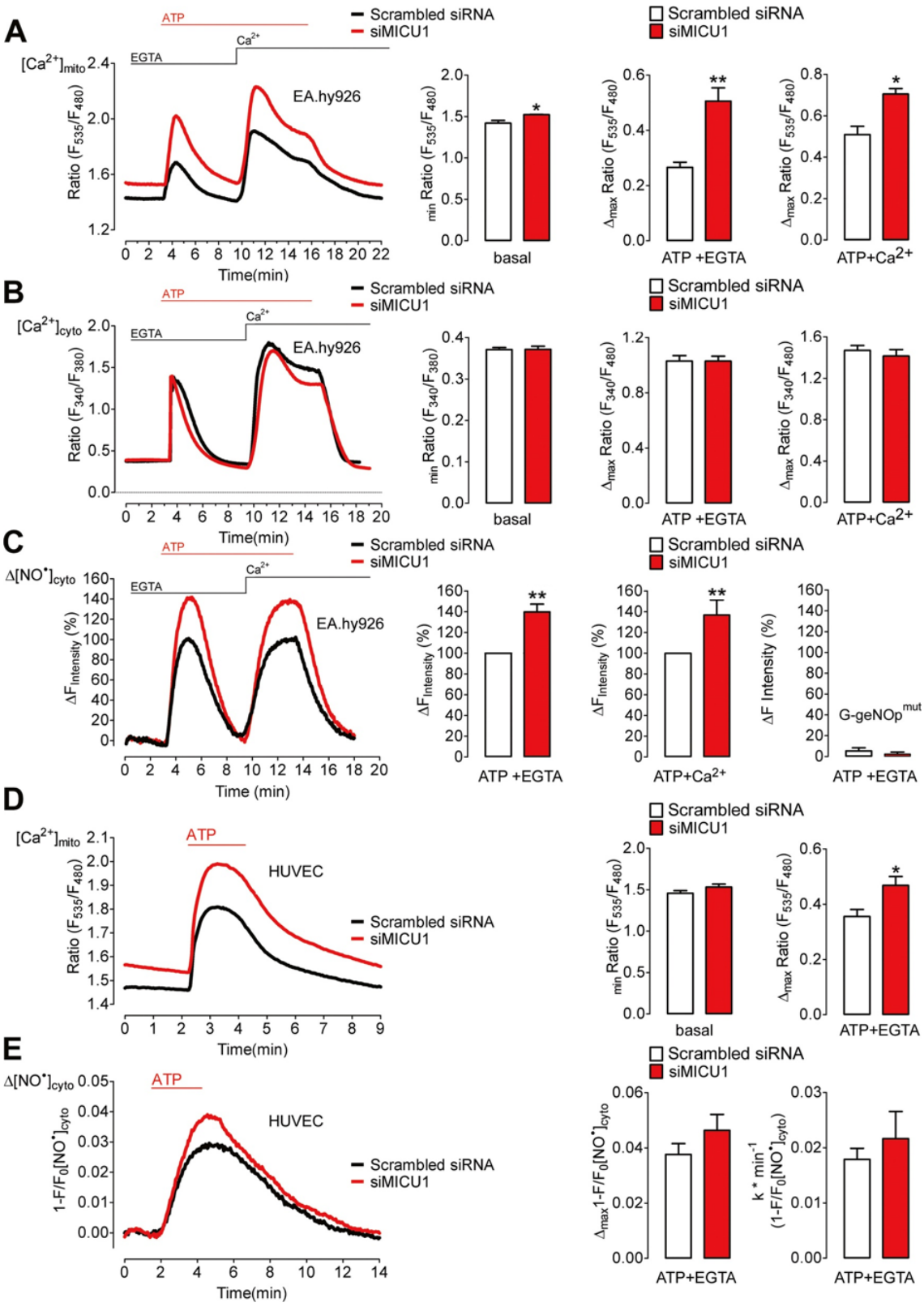
A
ATP
Ca2+
EGTA
[Ca2+]mito
EA.hy926
Ratio (F535/F480)
Time(min)
Scrambled siRNA
siMICU1
basal
ATP +EGTA
ATP+Ca2+
B
[Ca2+]cyto
Ratio (F340/F380)
Ratio (F340/F480)
C
Δ[NO•]cyto
ΔFIntensity (%)
Time (min)
ΔF Intensity (%)
G-geNOpmut
D
HUVEC
E
1-F/F0[NO•]cyto
k * min-1
(1-F/F0[NO•]cyto)

Figure 3.9 MICU1 knock-down increases $NO^{\bullet}$ signals in endothelial cells. (A) Representative mitochondrial Ca^{2+} signals obtained from siMICU1-ablated EA.hy926 cells (N = 6) and respective control cells (N = 6) upon stimulation with ATP (100 μM) in the absence and presence of extracellular Ca^{2+}. Left bars show ratios of basal $[Ca^{2+}]_{mito}$. Middle and right bars show the average $[Ca^{2+}]_{mito}$ amplitudes in response to ATP+EGTA and ATP+Ca^{2+}. (B) Average curves representing cytosolic Ca^{2+} transients of control cells (N = 6) and siMICU1-treated cells (N = 6) under the same experimental conditions. Left columns show $[Ca^{2+}]_{cyto}$ before ATP stimulation. Middle and right columns show maximal $[Ca^{2+}]_{cyto}$ upon ATP stimulation. (C) Representative curves of cytosolic $NO^{\bullet}$ signals in EA.hy926 cells in response to ATP-stimulated Ca^{2+} release and entry. $NO^{\bullet}$ amplitudes of scrambled siRNA- or siMICU1-treated cells are defined as 100% (scrambled siRNA, N = 17 and siMICU1, N = 16). Left and middle columns show respective average maximal $[NO^{\bullet}]_{cyto}$. Maximal fluorescence changes of G-geNOp^{mut}, under the same conditions and treatment, are shown in the right bar graph (control cells, N = 11 and siMICU1-treated cells, N = 8). (D) Representative mitochondrial Ca^{2+} signals of control HUVECs (N = 6) and the cells with MICU1 silencing (N = 6). Columns show $[Ca^{2+}]_{mito}$ before and after ATP stimulation. (E) Average $\Delta[NO^{\bullet}]_{cyto}$ of control HUVECs (N = 8) and cells treated with siMICU1 (N = 10) in response to ATP-containing Ca^{2+}-free HEPES buffer. Left and right columns show amplitudes and maximal slopes of G-geNOp signals. "*" for p value < 0.05 and "**" for p value < 0.01. [Reproduced from Charoensin S, Emrah E, Opelt M, et al. Intact mitochondrial Ca^{2+} uniport is essential for agonist-induced activation of endothelial $NO^{\bullet}$ synthase (eNOS). Free Radic Biol Med. 2017;102:248-59. (105), with permission of publisher Elsevier Inc. Copyright 2016.]

3.3 Mitochondrial depolarization causes reduced MCU-mediated Ca^{2+} uptake and subsequent $NO^{\bullet}$ reductions

As demonstrated that EMRE and MCU perturbation resulted in the negative effect on eNOS-dependent $NO^{\bullet}$ formation. Here, the confirmative experiments were performed in order to link the dependence of mitochondrial bioenergetics and Ca^{2+} uptake on $NO^{\bullet}$ production. The intact mitochondrial inner membrane potential ($\Delta\Psi_{mito}$) of EA.hy926 cells was collapsed using antimycin (5 μM) and oligomycin (1 μM). Antimycin inhibits electron transfer from cytochrome *b* to cytochrome c_1 (complex III), and oligomycin blocks ATP synthesis by inhibiting mitochondrial H-ATP synthase (complex V) (5, 101). Consequently, $\Delta\Psi_{mito}$ is depolarized, and Ca^{2+} uptake is halted (5, 101). Figure 3.10A and 3.10B represent average mitochondrial Ca^{2+} and TMRM signals of control (vehicle) and oligomycin/antimycin-treated cells. It was clearly observed that the depolarized mitochondria could significantly uptake less Ca^{2+} through their MCU complexes upon ATP-triggered ER Ca^{2+} release, in the absence and presence of entering Ca^{2+}, p = 0.0096 (in EGTA buffer) and p = 0.0159 (in Ca^{2+} buffer) (Figure 3.10A). A marked decline of average TMRM signal of treated cells (p = 0.0286 vs. control) occurred concomitantly with that of reduced Ca^{2+} uptake capacity of $\Delta\Psi_{mito}$-collapsed cells (Figure 3.10B). Figure 3.10C shows an average percentage of G-geNOp fluorescence signal upon ATP-induced mitochondrial Ca^{2+} uptake. Mitochondrial depolarization resulted in a significant inhibition of $NO^{\bullet}$ production compared to control cells, p = 0.0074 (in EGTA buffer) and p = 0.0200 (in Ca^{2+} buffer) (Figure 3.10C, left columns). The fluorescence signals of the G-geNOp^{mut}, however, were not affected during mitochondrial depolarization and independent of the presence of Ca^{2+} (Figure 3.10C, right columns). However, under the same experimental conditions, cytosolic Ca^{2+} levels observed in $\Delta\Psi_{mito}$-collapsed cells were only partially reduced during Ca^{2+} addition (Figure 3.10D). Therefore, these results point out that the intact mitochondrial Ca^{2+} uptake and mitochondrial bioenergetics involve in eNOS-catalyzed $NO^{\bullet}$ formation.

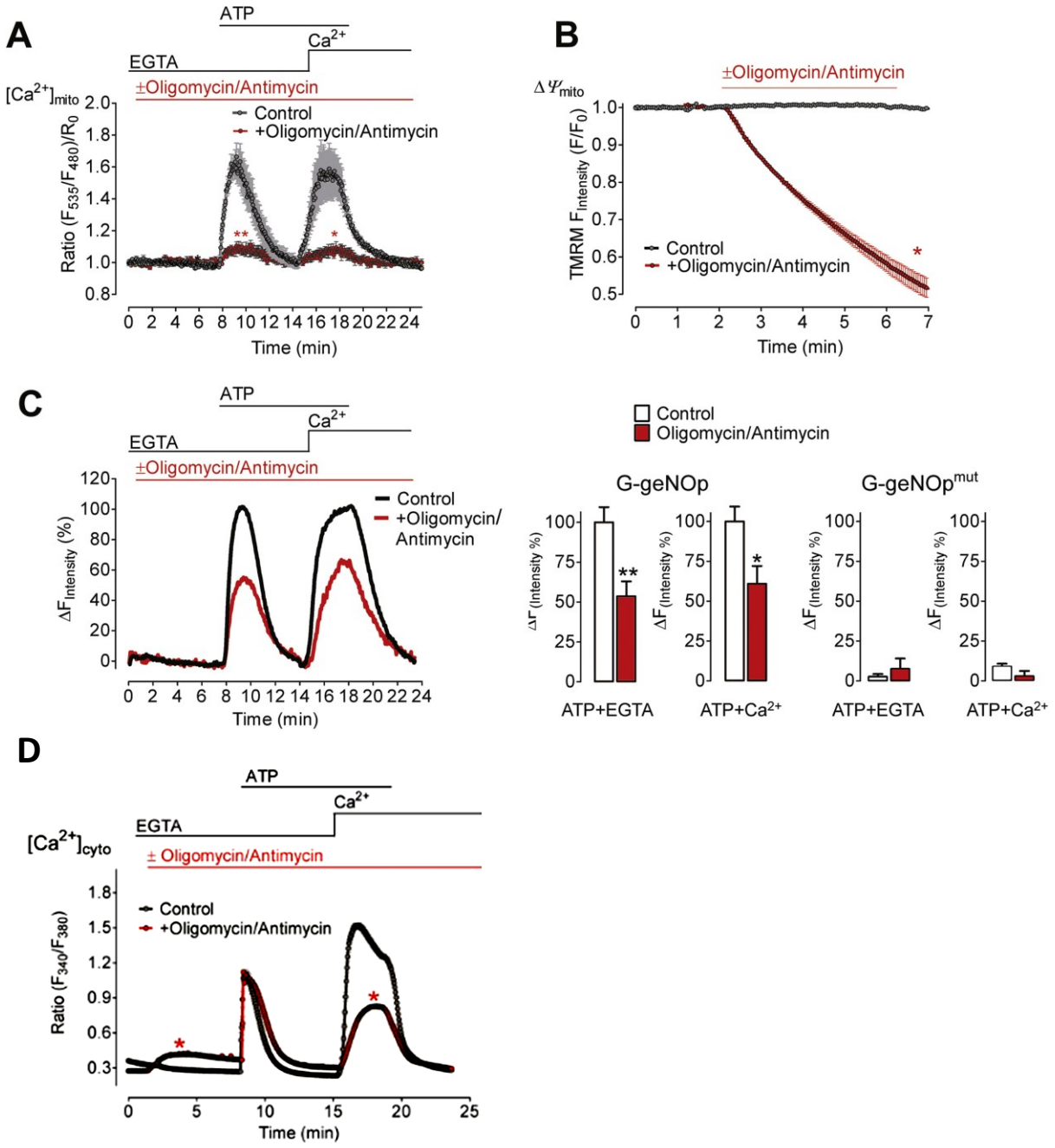

Figure 3.10 Mitochondrial depolarization reduces Ca^{2+}-triggered $NO^{\bullet}$ formation. (A) Average mitochondrial Ca^{2+} signals of control EA.hy926 cells (N = 8) and the cells treated with antimycin (5 μM) and oligomycin (1 μM) (N = 12) in response to ATP (100 μM) (B) Average TMRM fluorescence signals of control conditions (N = 6) and upon oligomycin and antimycin treatment (N = 6). (C) Average $\Delta[NO^{\bullet}]_{cyto}$ of control cells (N = 11) and treated-cells (N = 9) upon ATP-stimulated Ca^{2+} release and entry. Maximal signals under control conditions were defined as 100% during Ca^{2+} release and entry (middle bars). Right bars show

maximal fluorescence changes of G-geNOp^{mut} of control cells (N = 6) and treated-cells (N = 6). (D) Average fura-2 signals showing ATP-triggered cytosolic Ca^{2+} transients in EA.hy926 cells (control, N = 6 and treated-cells, N = 6). "*" for *p* value < 0.05 and "**" for *p* value < 0.01. [Reproduced from Charoensin S, Emrah E, Opelt M, et al. Intact mitochondrial Ca^{2+} uniport is essential for agonist-induced activation of endothelial $NO^{\bullet}$ synthase (eNOS). Free Radic Biol Med. 2017;102:248-59. (105), with permission of publisher Elsevier Inc. Copyright 2016.]

3.4 eNOS expressions in MCU complex-perturbed EA.hy926 cells

It has been reported that phosphorylation is one of the important post-translational modifications that modulates eNOS activity (10, 100). This molecular mechanism can result in both stimulatory or inhibitory effect to the enzyme (10, 113). In this study, the endogenous levels of total eNOS protein and the expressions of its phosphorylated form (peNOS) were determined to find out whether perturbation of MCU complex affected eNOS phosphorylation at serine1177. For this purpose, EA.hy926 cells were treated with ATP for 3 or 5 minutes. Western blot analysis clearly showed that expression levels of peNOS in cells treated with either scrambled siRNA or siRNAs against EMRE/MCU or MICU1 were increased after ATP treatment (Figure 3.11A). The ratios of phosphorylated to total eNOS protein (peNOS/eNOS) of knocked-down cells were indifferent upon ATP-triggered mitochondrial Ca^{2+} sequestration (3 or 5 minutes of incubations) (Figure 3.11B). This result indicates that the mitochondrial Ca^{2+} signals do not influence eNOS phosphorylation at serine 1177. Furthermore, this result also implies that the increased $NO^{\bullet}$ production in this cell type might be due to an inherent mitochondrial Ca^{2+} signaling following matrix Ca^{2+} augmentation within endothelial mitochondria.

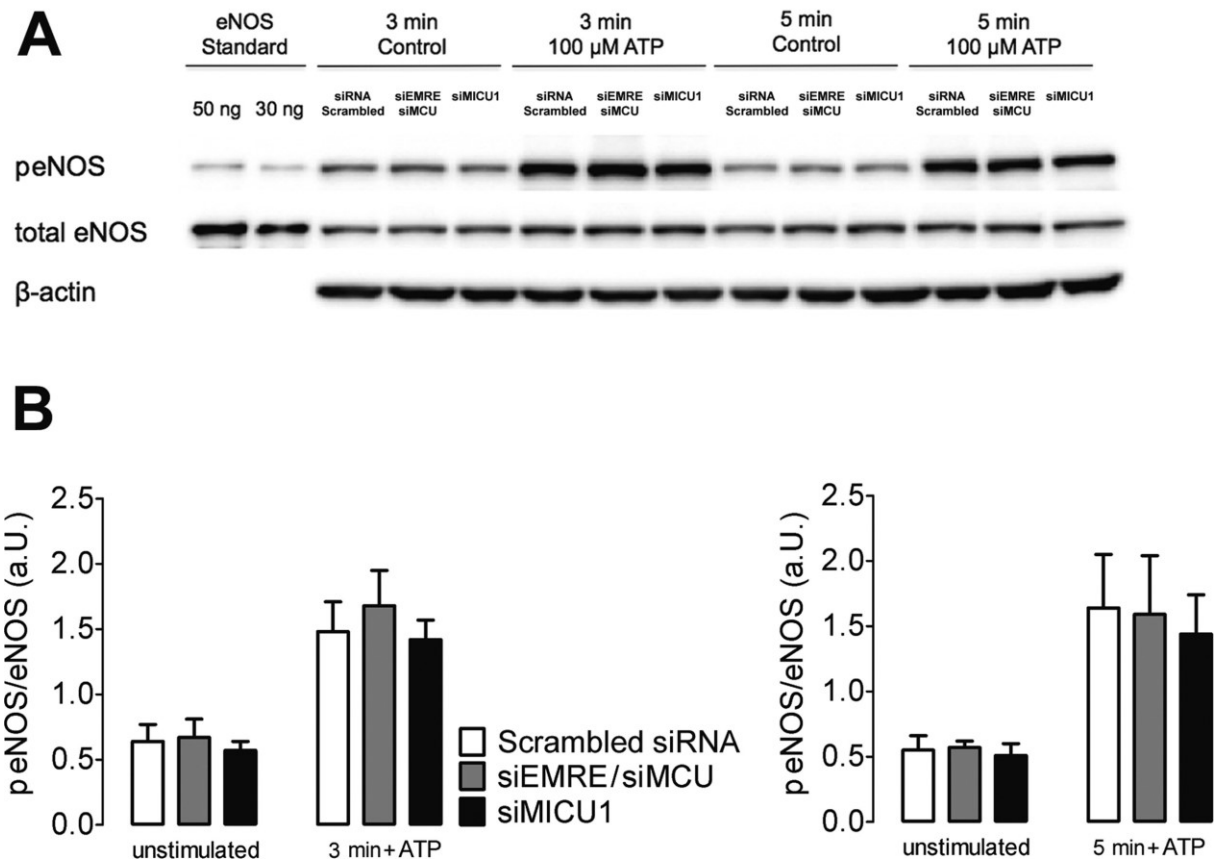

Figure 3.11 EMRE/MCU and MICU1 knock-down does not affect eNOS expression levels and phosphorylation state in EA.hy926 cells. (A) Expression of total eNOS and its phosphorylated form (peNOS) in EA.hy926 cells transfected with either scrambled siRNA and siRNA against MCU, EMRE and MICU1 in response to ATP (100 μM) for 3 or 5 minutes (N = 3 for all conditions). Purified human eNOS was used as standard protein. β-actin was used as internal control for normalization. (B) Average ratios of peNOS/eNOS of EA.hy926 cells after ATP treatments. [Reproduced from Charoensin S, Emrah E, Opelt M, et al. Intact mitochondrial Ca^{2+} uniport is essential for agonist-induced activation of endothelial $NO^{\bullet}$ synthase (eNOS). Free Radic Biol Med. 2017;102:248-59. (105), with permission of publisher Elsevier Inc. Copyright 2016.]

3.5 Investigation of $NO^{\bullet}$ dynamics in eNOS-expressing HEK293 cells

HEK293 cells were transiently transfected with G-geNOp alone or in combination with eNOS-RFP. Figure 3.12A illustrates a confocal image of eNOS-RFP expressing HEK293 cells in which the enzyme immensely located at the plasma membrane, with lesser extent in the intracellular vesicles but not within mitochondria. Upon ATP-triggered Ca^{2+} release from endoplasmic reticulum, the co-transfected HEK293 cells produced a significant amount of $NO^{\bullet}$ over the control cells ($p = 0.0005$) in a short period of time (Figure 3.12B, columns). To check G-geNOp responsibility, sodium nitroprusside (SNP) was added at the end of the recordings and the HEK293 cells in both conditions could sense $NO^{\bullet}$ almost immediately after SNP addition (Figure 3.12B). Further experiments were carried out to manipulate MCU-mediated mitochondrial Ca^{2+} uptake on eNOS-dependent $NO^{\bullet}$ production. Silencing of both EMRE and MCU in HEK293 cells significantly reduced ATP-evoked mitochondrial Ca^{2+} accumulation ($p = 0.0145$) (Figure 3.12C, right columns). Conversely, MICU1 knocked down cells considerably accumulated more Ca^{2+} under basal condition ($p = 0.0004$) and in response to ATP stimulation ($p = 0.0152$) (Figure 3.12C, left and right columns, respectively). There was no alteration of respective cytosolic Ca^{2+} transients (Figure 3.12D). By taking up less Ca^{2+} into their matrix, the siEMRE/siMCU-transfected HEK293 cells expressing eNOS-RFP resulted in a significant decline of average $NO^{\bullet}$ signal ($p = 0.0005$ vs. control) (Figure 3.12E, right columns). Yet, siMICU1-transfected cells only showed a slight $NO^{\bullet}$ increase. These results, particularly that observed in the cells with EMRE and MCU silencing, were consistent with those observed in EA.hy926 cells and primary HUVECs. Based on the HEK293 cells' experiments, it is possible that less or poor matrix Ca^{2+} accumulation might cause an inadequate support of eNOS-requiring factors for $NO^{\bullet}$ production and availability.

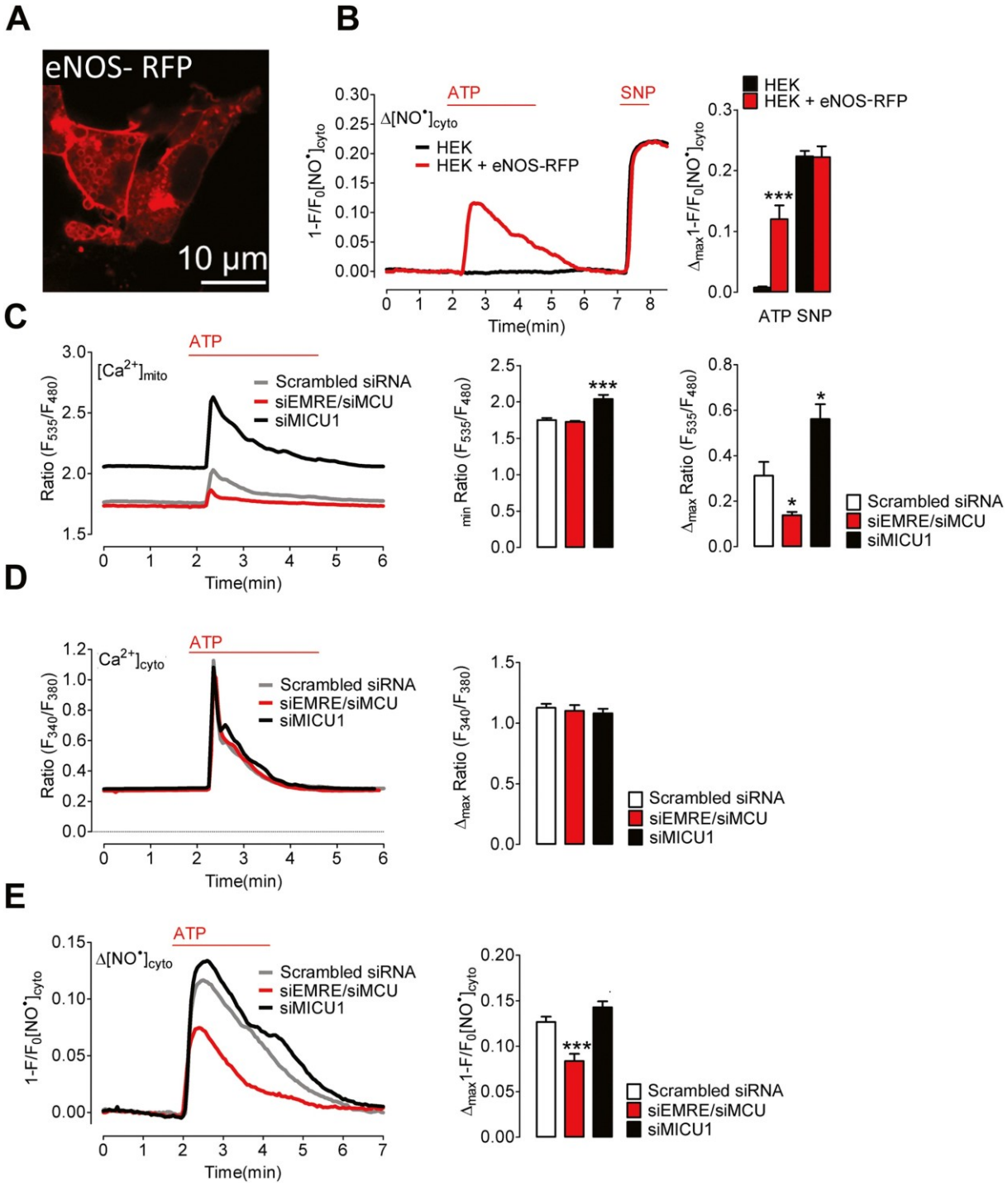

Figure 3.12 Mitochondrial Ca^{2+} uptake controls $NO^{\bullet}$ formation in HEK293 cells expressing eNOS-RFP. (A) Representative image showing plasma membrane localization of eNOS-RFP in HEK293 cells. (B) Average cytosolic $NO^{\bullet}$ signals of control cells (N = 5) and cells expressing eNOS-RFP (N = 3) upon 100 μM ATP-stimulated Ca^{2+} release. Columns show average maximal $[NO^{\bullet}]_{cyto}$ after ATP and sodium nitroprusside (SNP, 1 mM) treatment.

(C) Average mitochondrial Ca^{2+} signals in eNOS-expressing HEK293 cells with or without siRNA transfections in response to ATP-trigger Ca^{2+} release (scrambled siRNA, N = 8, siEMRE/siMCU, N = 8 and siMICU1, N = 7). Left bars show average $[Ca^{2+}]_{mito}$ before ATP stimulation and right bars after ATP stimulation. (D) Respective $[Ca^{2+}]_{cyto}$ of eNOS-expressing HEK293 cells (scrambled siRNA, N = 3, siEMRE/siMCU, N = 3 and siMICU1, N = 4). Bars represent maximal $[Ca^{2+}]_{cyto}$ upon ATP treatment. (E) Curves representing average $\Delta[NO^{\bullet}]_{cyto}$ of control cells and siRNA-transfected HEK293 cells (scrambled siRNA, N = 9, siEMRE/siMCU, N = 11 and siMICU1, N = 8). Bars show average amplitudes of G-geNOp fluorescence signals. "*" for p value < 0.05 and "***" for p value less than 0.001. [Reproduced from Charoensin S, Emrah E, Opelt M, et al. Intact mitochondrial Ca^{2+} uniport is essential for agonist-induced activation of endothelial $NO^{\bullet}$ synthase (eNOS). Free Radic Biol Med. 2017;102:248-59. (105), with permission of publisher Elsevier Inc. Copyright 2016.]

CHAPTER 4

DISCUSSION

According to the present dissertation work, the significant role of MCU-mediated mitochondrial Ca^{2+} uptake and signaling on eNOS-dependent $NO^{\bullet}$ production within endothelial cells was originally reported. Outputs of the present study bring up a better understanding on how mitochondrial Ca^{2+} associates with eNOS function and $NO^{\bullet}$ synthesis under purinergic activation and IP_3 signaling.

There is an attempt to better understand the involvement of mitochondria in endothelial and cardiac $NO^{\bullet}$ availability (101, 114, 115). The distinct experiment using permeabilized calf pulmonary artery endothelial cells has demonstrated that, upon increased Ca^{2+} concentration, the $NO^{\bullet}$ signals detected by fluorescent dye DAF-2-DA elevate despite using cell permeabilizing agent and unspecific $NO^{\bullet}$ probe (101, 115, 116). According to that, the exact molecular events respective to $NO^{\bullet}$ production were not appropriately manipulated because of possible interfered enzyme/protein structure and function and inherent pitfalls from a probe's chemical property (116). In the recent years, the MCU complex (MCU and EMRE) and its associated proteins (MICU1/2, MCUR1 and MCUb) have been identified (43, 50, 51). There are extensive research interests that aim to manipulate these mitochondrial inner proteins particularly in investigating their biochemical functions in physiological and pathophysiological conditions (42, 72, 117). Therefore, the present study sought to investigate the significance of mitochondrial Ca^{2+} signal on endothelial $NO^{\bullet}$ dynamics by furthering the recent knowledge on mitochondrial Ca^{2+} uptake machinery along with the use of the novel $NO^{\bullet}$ probe (geNOp) (104). The present work showed that, upon fluorescence quenching of G-geNOp, the $NO^{\bullet}$ dynamics increased when EA.hy926 cells were treated with IP_3-generating agonist (ATP) (Figure 3.1C and 3.1D). The dynamic changes were coincident with rapidly augmented intracellular Ca^{2+} transients (Figure 3.1D). Notably, EA.hy926 cells had faster $NO^{\bullet}$ kinetics compared to HUVECs (Figure 3.8C). It might be due to the differences in subcellular localization, expression level and post-translational control of eNOS between the primary cell and the cell line (97, 117, 118). These results together with previous reports suggest that the geNOp technology is suitable for investigation of endothelial $NO^{\bullet}$ dynamics (104). By silencing EMRE and MCU in EA.hy926 cells, endothelial mitochondria could uptake less

Ca^{2+} into the matrix (Figure 3.7A), while cytosolic Ca^{2+} levels remained unchanged (Figure 3.7B), which is in line with previous reports (28, 76, 84, 108). The decline in mitochondrial Ca^{2+} accumulation under purinergic stimulation of Ca^{2+} release resulted in the reduced capacity of eNOS in producing $NO^{\bullet}$ (Figure 3.7C and 3.7D). This indicates that mitochondrial Ca^{2+} signal was biochemically significant for the production of this vasodilatory substance. Furthermore, the experiments conducted in primary HUVECs and HEK293 cells showed very consistent results in $NO^{\bullet}$ dynamics with the current finding found in EA.hy926 cells (Figure 3.8E and 3.12E). Considering MCU complex-mediated Ca^{2+} uptake into mitochondria in each cell type (Figure 3.7A, 3.8B and 3.12C), it is clear that this uniport complex not only mediates Ca^{2+} transport across inner membrane but also shapes Ca^{2+} signals inside and outside the mitochondria (119). With that, it governs mitochondrial Ca^{2+} signaling and relevant Ca^{2+}-sensitive pathways (38, 120, 121). Manipulation of mitochondrial respiration using pharmacological compounds capable of blocking complex III and F1/F0 ATP synthase caused the bioenergetic collapse and subsequent mitochondrial depolarization (Figure 3.10B). Consequently, mitochondrial Ca^{2+} uptake capacity was disrupted due to an electrogenic disturbance in intermembrane space (36). It has been demonstrated that the calf pulmonary artery endothelial cells and EA.hy926 cells fail to sequester increased intracellular Ca^{2+} when the mitochondria are depolarized by OXPHOS inhibitor or uncoupling agent FCCP (101). Dissipation of mitochondrial membrane potential altered dynamics of both mitochondrial Ca^{2+} and cytosolic $NO^{\bullet}$ (Figure 3.10A and 3.10C). These results emphasize that intact mitochondria are essential for endothelial $NO^{\bullet}$ synthesis. Therefore, based on the present finding, the appropriate mitochondrial and cytoplasmic Ca^{2+} signals closely associate with endothelial $NO^{\bullet}$ homeostasis.

According to the previous publications, the $NO^{\bullet}$ dynamics in permeabilized endothelial cells was investigated without intrinsic intracellular Ca^{2+} signaling but with extracellular Ca^{2+} addition (5, 101). So, obtained results are less pronounced, and the effect of mitochondrial Ca^{2+} uptake on $NO^{\bullet}$ formation in this cell type is still elusive. In terms of physiological conditions and high-quality imaging, siRNA against MICU1 and G-geNOp were preferentially applied for visualization of $NO^{\bullet}$ dynamics in response to ATP-evoked mitochondrial Ca^{2+} accumulation. Mitochondria of EA.hy926, HUVECs and HEK293 cells were found to take up more Ca^{2+} into their matrices upon Ca^{2+} release from internal store (Figure 3.9A, 3.9D and

3.12C). Interestingly, under this condition, cytosolic $NO^{\bullet}$ increasingly formed in EA.hy926 cells up to 40% (Figure 3.9C), only slight amounts in HUVECs and HEK239 cells (Figure 3.9E and 3.12E). Positive effect of increased mitochondrial Ca^{2+} on $NO^{\bullet}$ augmentation observed in MICU1-silenced cells was in agreement with seminal publications (5, 101). Elaboration on this finding is seemingly relevant to mitochondrial support when Ca^{2+} accumulates more in the matrix. It has been reported that several mitochondrial enzymes are dependent on matrix Ca^{2+}, and their activities are enhanced upon more Ca^{2+} accumulation (signal) within mitochondrial matrix (16, 121, 122). Moreover, the result is consistent with the previous concept of Ca^{2+}-dependent mitochondria-specific NOS despite limited clear proof of its existence in endothelium (16, 122-124). It might be that the key mitochondrial Ca^{2+}-sensitive enzymes in bioenergetic pathway and/or mitochondria-derived cofactors contributed to the significant $NO^{\bullet}$ formation, apart from cytosolic Ca^{2+}-mediated eNOS activation (16, 40, 121, 122). Besides, analyses of eNOS and phospho-eNOS expression revealed no association between EMRE/MCU or MICU1 knockdown and phosphorylating level of the enzyme even when EA.hy926 cells were treated with ATP (Figure 3.11A and 3.11B). Only the ATP treatment that enhanced the phosphorylation of the enzyme, which is in line with the previous reports describing the association between Ca^{2+}/CaM complex binding to eNOS and enhanced enzymatic activity (125, 126). Upon binding to its conserved domain located on eNOS, this complex facilitates the electron flux from the reductase to the oxygenase domain and triggers conformational change for phosphorylation on tyrosine residues (6, 9). Presumably, some known kinase pathways (e.g., AMPK, PKC, or PI3K/PKB) are downstream targets capable of phosphorylating eNOS at sensitive serine (89, 113, 127, 128). Based on the present study, it is obvious that the augmented mitochondrial Ca^{2+} uptake is directly involved in eNOS-dependent $NO^{\bullet}$ production.

In conclusion, by utilizing the unprecedented G-geNOp technology and manipulating mitochondrial Ca^{2+} uptake machinery, the present dissertation work reveals that mitochondrial Ca^{2+} signal is indispensable for endothelial $NO^{\bullet}$ generation. MICU1 silencing promotes mitochondrial Ca^{2+} accumulation and $NO^{\bullet}$ synthesis. While, MCU/EMRE knock-down reduces $NO^{\bullet}$ content due to less matrix Ca^{2+} sequestration. Pronounced research significance arising from the dissertation is that the increased Ca^{2+} uptake by mitochondria promotes Ca^{2+}-triggered $NO^{\bullet}$ formation. MCU complex may represent its new regulatory function on

mitochondrially-regulated eNOS-mediated $NO^{\bullet}$ production. Therefore, targeting endothelial mitochondrial Ca^{2+} signal to maximize eNOS function may restore vascular homeostasis across spectrum of vascular disease.

BIBLIOGRAPHY

1. Kishimoto J, Spurr N, Liao M, Lizhi L, Emson P, Xu W. Localization of brain nitric oxide synthase (NOS) to human chromosome 12. Genomics. 1992;14(3):802-4.
2. Kroncke KD, Fehsel K, Kolb-Bachofen V. Inducible nitric oxide synthase and its product nitric oxide, a small molecule with complex biological activities. Biol Chem Hoppe Seyler. 1995;376(6):327-43.
3. Förstermann U, Closs EI, Pollock JS, Nakane M, Schwarz P, Gath I, et al. Nitric oxide synthase isozymes. Characterization, purification, molecular cloning, and functions. Hypertension. 1994;23(6 Pt 2):1121-31.
4. Carreras MC, Franco MC, Finocchietto PV, Converso DP, Antico Arciuch VG, Holod S, et al. The biological significance of mtNOS modulation. Front Biosci. 2007;12:1041-8.
5. Dedkova EN, Blatter LA. Modulation of mitochondrial Ca^{2+} by nitric oxide in cultured bovine vascular endothelial cells. Am J Physiol Cell Physiol. 2005;289(4):C836-45.
6. Zhao Y, Vanhoutte PM, Leung SW. Vascular nitric oxide: beyond eNOS. J Pharmacol Sci. 2015;129(2):83-94.
7. Weissman BA, Jones CL, Liu Q, Gross SS. Activation and inactivation of neuronal nitric oxide synthase: characterization of Ca^{2+}-dependent [125I] calmodulin binding. Eur J Pharmacol. 2002;435(1):9-18.
8. Vanhoutte PM, Zhao Y, Xu A, Leung SW. Thirty years of saying NO: sources, fate, actions, and misfortunes of the endothelium-derived vasodilator mediator. Circ Res. 2016;119(2):375-96.
9. Förstermann U, Sessa WC. Nitric oxide synthases: regulation and function. Eur Heart J. 2012;33(7):829-37, 37a-37d.
10. Kolluru GK, Siamwala JH, Chatterjee S. eNOS phosphorylation in health and disease. Biochimie. 2010;92(9):1186-98.
11. Denninger JW, Marletta MA. Guanylate cyclase and the NO/cGMP signaling pathway. Biochim Biophys Acta. 1999;1411(2-3):334-50.
12. Carvajal JA, Germain AM, Huidobro-Toro JP, Weiner CP. Molecular mechanism of cGMP-mediated smooth muscle relaxation. J Cell Physiol. 2000;184(3):409-20.
13. Vanhoutte PM, Shimokawa H, Tang EH, Feletou M. Endothelial dysfunction and vascular disease. Acta Physiol (Oxf). 2009;196(2):193-222.

14. Hagan G, Pepke-Zaba J. Pulmonary hypertension, nitric oxide and nitric oxide-releasing compounds. Expert Rev Respir Med. 2011;5(2):163-71.

15. Sarti P, Forte E, Mastronicola D, Giuffre A, Arese M. Cytochrome *c* oxidase and nitric oxide in action: molecular mechanisms and pathophysiological implications. Biochim Biophys Acta. 2012;1817(4):610-9.

16. Traaseth N, Elfering S, Solien J, Haynes V, Giulivi C. Role of calcium signaling in the activation of mitochondrial nitric oxide synthase and citric acid cycle. Biochim Biophys Acta. 2004;1658(1-2):64-71.

17. Giulivi C, Kato K, Cooper CE. Nitric oxide regulation of mitochondrial oxygen consumption I: cellular physiology. Am J Physiol Cell Physiol. 2006;291(6):C1225-31.

18. Lipina C, Hundal HS. The endocannabinoid system: 'NO' longer anonymous in the control of nitrergic signalling? J Mol Cell Biol. 2017;9(2):91-103.

19. Umbrello M, Dyson A, Feelisch M, Singer M. The key role of nitric oxide in hypoxia: hypoxic vasodilation and energy supply-demand matching. Antioxid Redox Signal. 2013;19(14):1690-710.

20. Cooper CE, Giulivi C. Nitric oxide regulation of mitochondrial oxygen consumption II: Molecular mechanism and tissue physiology. Am J Physiol Cell Physiol. 2007;292(6):C1993-2003.

21. San Martin A, Arce-Molina R, Galaz A, Perez-Guerra G, Barros LF. Nanomolar nitric oxide concentrations quickly and reversibly modulate astrocytic energy metabolism. J Biol Chem. 2017;292(22):9432-8.

22. Iglesias DE, Bombicino SS, Valdez LB, Boveris A. Nitric oxide interacts with mitochondrial complex III producing antimycin-like effects. Free Radic Biol Med. 2015;89:602-13.

23. Brini M, Cali T, Ottolini D, Carafoli E. Intracellular calcium homeostasis and signaling. Met Ions Life Sci. 2013;12:119-68.

24. Carafoli E, Krebs J. Why calcium? How calcium became the best communicator. J Biol Chem. 2016;291(40):20849-57.

25. Marshall CB, Nishikawa T, Osawa M, Stathopulos PB, Ikura M. Calmodulin and STIM proteins: two major calcium sensors in the cytoplasm and endoplasmic reticulum. Biochem Biophys Res Commun. 2015;460(1):5-21.

26. Cai H, Liu D, Garcia JG. CaM Kinase II-dependent pathophysiological signalling in endothelial cells. Cardiovasc Res. 2008;77(1):30-4.

27. Greif DM, Sacks DB, Michel T. Calmodulin phosphorylation and modulation of endothelial nitric oxide synthase catalysis. Proc Natl Acad Sci U S A. 2004;101(5):1165-70.

28. Deak AT, Blass S, Khan MJ, Groschner LN, Waldeck-Weiermair M, Hallstrom S, et al. IP_3-mediated STIM1 oligomerization requires intact mitochondrial Ca^{2+} uptake. J Cell Sci. 2014;127(Pt 13):2944-55.

29. Graier WF, Frieden M, Malli R. Mitochondria and Ca^{2+} signaling: old guests, new functions. Pflugers Arch. 2007;455(3):375-96.

30. Burnstock G. Purinergic signalling: from discovery to current developments. Exp Physiol. 2014;99(1):16-34.

31. Burnstock G, Brouns I, Adriaensen D, Timmermans JP. Purinergic signaling in the airways. Pharmacol Rev. 2012;64(4):834-68.

32. Burnstock G, Knight GE. Cellular distribution and functions of P2 receptor subtypes in different systems. Int Rev Cytol. 2004;240:31-304.

33. Burnstock G. Dual control of vascular tone and remodelling by ATP released from nerves and endothelial cells. Pharmacol Rep. 2008;60(1):12-20.

34. Malli R, Frieden M, Osibow K, Zoratti C, Mayer M, Demaurex N, et al. Sustained Ca^{2+} transfer across mitochondria is essential for mitochondrial Ca^{2+} buffering, store-operated Ca^{2+} entry, and Ca^{2+} store refilling. J Biol Chem. 2003;278(45):44769-79.

35. Di Giuro CML, Shrestha N, Malli R, Groschner K, van Breemen C, Fameli N. Na^{+}/Ca^{2+} exchangers and Orai channels jointly refill endoplasmic reticulum (ER) Ca^{2+} via ER nanojunctions in vascular endothelial cells. Pflugers Arch - Eur J Physiol. 2017;469(10):1287-99.

36. Vishnu N, Jadoon Khan M, Karsten F, Groschner LN, Waldeck-Weiermair M, Rost R, et al. ATP increases within the lumen of the endoplasmic reticulum upon intracellular Ca^{2+} release. Mol Biol Cell. 2014;25(3):368-79.

37. Tran QK, Watanabe H. Calcium signalling in the endothelium. Handb Exp Pharmacol. 2006(176 Pt 1):145-87.

38. Bhosale G, Sharpe JA, Sundier SY, Duchen MR. Calcium signaling as a mediator of cell energy demand and a trigger to cell death. Ann N Y Acad Sci. 2015;1350:107-16.

39. Rafikov R, Fonseca FV, Kumar S, Pardo D, Darragh C, Elms S, et al. eNOS activation and NO function: structural motifs responsible for the posttranslational control of endothelial nitric oxide synthase activity. J Endocrinol. 2011;210(3):271-84.

40. Luckhoff A, Pohl U, Mulsch A, Busse R. Differential role of extra- and intracellular calcium in the release of EDRF and prostacyclin from cultured endothelial cells. Br J Pharmacol. 1988;95(1):189-96.

41. Burnstock G. Purinergic signaling and vascular cell proliferation and death. Arterioscler Thromb Vasc Biol. 2002;22(3):364-73.

42. Mammucari C, Raffaello A, Vecellio Reane D, Rizzuto R. Molecular structure and pathophysiological roles of the mitochondrial calcium uniporter. Biochim Biophys Acta. 2016;1863(10):2457-64.

43. Mallilankaraman K, Doonan P, Cardenas C, Chandramoorthy HC, Muller M, Miller R, et al. MICU1 is an essential gatekeeper for MCU-mediated mitochondrial Ca^{2+} uptake that regulates cell survival. Cell. 2012;151(3):630-44.

44. Mallilankaraman K, Cardenas C, Doonan PJ, Chandramoorthy HC, Irrinki KM, Golenar T, et al. MCUR1 is an essential component of mitochondrial Ca^{2+} uptake that regulates cellular metabolism. Nat Cell Biol. 2015;17(7):953.

45. Del Arco A, Contreras L, Pardo B, Satrustegui J. Calcium regulation of mitochondrial carriers. Biochim Biophys Acta. 2016;1863(10):2413-21.

46. Luongo TS, Lambert JP, Yuan A, Zhang X, Gross P, Song J, et al. The mitochondrial calcium uniporter matches energetic supply with cardiac workload during stress and modulates permeability transition. Cell Rep. 2015;12(1):23-34.

47. Alam MR, Groschner LN, Parichatikanond W, Kuo L, Bondarenko AI, Rost R, et al. Mitochondrial Ca^{2+} uptake 1 (MICU1) and mitochondrial Ca^{2+} uniporter (MCU) contribute to metabolism-secretion coupling in clonal pancreatic beta-cells. J Biol Chem. 2012;287(41):34445-54.

48. Murgia M, Giorgi C, Pinton P, Rizzuto R. Controlling metabolism and cell death: at the heart of mitochondrial calcium signalling. J Mol Cell Cardiol. 2009;46(6):781-8.

49. De Stefani D, Raffaello A, Teardo E, Szabo I, Rizzuto R. A forty-kilodalton protein of the inner membrane is the mitochondrial calcium uniporter. Nature. 2011;476(7360):336-40.

50. Baughman JM, Perocchi F, Girgis HS, Plovanich M, Belcher-Timme CA, Sancak Y, et al. Integrative genomics identifies MCU as an essential component of the mitochondrial calcium uniporter. Nature. 2011;476(7360):341-5.

51. Sancak Y, Markhard AL, Kitami T, Kovacs-Bogdan E, Kamer KJ, Udeshi ND, et al. EMRE is an essential component of the mitochondrial calcium uniporter complex. Science. 2013;342(6164):1379-82.

52. Vais H, Tanis JE, Muller M, Payne R, Mallilankaraman K, Foskett JK. MCUR1, CCDC90A, is a regulator of the mitochondrial calcium uniporter. Cell Metab. 2015;22(4):533-5.

53. Perocchi F, Gohil VM, Girgis HS, Bao XR, McCombs JE, Palmer AE, et al. MICU1 encodes a mitochondrial EF hand protein required for Ca^{2+} uptake. Nature. 2010;467(7313):291-6.

54. Plovanich M, Bogorad RL, Sancak Y, Kamer KJ, Strittmatter L, Li AA, et al. MICU2, a paralog of MICU1, resides within the mitochondrial uniporter complex to regulate calcium handling. PLoS One. 2013;8(2):e55785.

55. Raffaello A, De Stefani D, Sabbadin D, Teardo E, Merli G, Picard A, et al. The mitochondrial calcium uniporter is a multimer that can include a dominant-negative pore-forming subunit. EMBO J. 2013;32(17):2362-76.

56. Rizzuto R, De Stefani D, Raffaello A, Mammucari C. Mitochondria as sensors and regulators of calcium signalling. Nat Rev Mol Cell Biol. 2012;13(9):566-78.

57. Behringer EJ, Segal SS. Membrane potential governs calcium influx into microvascular endothelium: integral role for muscarinic receptor activation. J Physiol. 2015;593(20):4531-48.

58. Luongo TS, Lambert JP, Gross P, Nwokedi M, Lombardi AA, Shanmughapriya S, et al. The mitochondrial Na^+/Ca^{2+} exchanger is essential for Ca^{2+} homeostasis and viability. Nature. 2017;545(7652):93-7.

59. Brand MD. The stoichiometry of the exchange catalysed by the mitochondrial calcium/sodium antiporter. Biochem J. 1985;229(1):161-6.

60. Jiang D, Zhao L, Clapham DE. Genome-wide RNAi screen identifies Letm1 as a mitochondrial Ca^{2+}/H^+ antiporter. Science. 2009;326(5949):144-7.

61. Hashimi H, McDonald L, Stribrna E, Lukes J. Trypanosome Letm1 protein is essential for mitochondrial potassium homeostasis. J Biol Chem. 2013;288(37):26914-25.

62. Palty R, Silverman WF, Hershfinkel M, Caporale T, Sensi SL, Parnis J, et al. NCLX is an essential component of mitochondrial Na^+/Ca^{2+} exchange. Proc Natl Acad Sci U S A. 2010;107(1):436-41.

63. De Stefani D, Patron M, Rizzuto R. Structure and function of the mitochondrial calcium uniporter complex. Biochim Biophys Acta. 2015;1853(9):2006-11.

64. Bononi A, Missiroli S, Poletti F, Suski JM, Agnoletto C, Bonora M, et al. Mitochondria-associated membranes (MAMs) as hotspot Ca^{2+} signaling units. Adv Exp Med Biol. 2012;740:411-37.

65. Patergnani S, Suski JM, Agnoletto C, Bononi A, Bonora M, De Marchi E, et al. Calcium signaling around mitochondria associated membranes (MAMs). Cell Commun Signal. 2011;9:19.

66. Kamer KJ, Sancak Y, Mootha VK. The uniporter: from newly identified parts to function. Biochem Biophys Res Commun. 2014;449(4):370-2.

67. Mammucari C, Gherardi G, Zamparo I, Raffaello A, Boncompagni S, Chemello F, et al. The mitochondrial calcium uniporter controls skeletal muscle trophism *in vivo*. Cell Rep. 2015;10(8):1269-79.

68. Tosatto A, Sommaggio R, Kummerow C, Bentham RB, Blacker TS, Berecz T, et al. The mitochondrial calcium uniporter regulates breast cancer progression via HIF-1alpha. EMBO Mol Med. 2016;8(5):569-85.

69. Groschner LN, Alam MR, Graier WF. Metabolism-secretion coupling and mitochondrial calcium activities in clonal pancreatic beta-cells. Vitam Horm. 2014;95:63-86.

70. Dong Z, Shanmughapriya S, Tomar D, Siddiqui N, Lynch S, Nemani N, et al. Mitochondrial Ca^{2+} uniporter is a mitochondrial luminal redox sensor that augments MCU channel activity. Mol Cell. 2017;65(6):1014-28.e7.

71. Fieni F, Lee SB, Jan YN, Kirichok Y. Activity of the mitochondrial calcium uniporter varies greatly between tissues. Nat Commun. 2012;3:1317.

72. Pan X, Liu J, Nguyen T, Liu C, Sun J, Teng Y, et al. The physiological role of mitochondrial calcium revealed by mice lacking the mitochondrial calcium uniporter. Nat Cell Biol. 2013;15(12):1464-72.

73. Vais H, Mallilankaraman K, Mak DO, Hoff H, Payne R, Tanis JE, et al. EMRE is a matrix Ca^{2+} sensor that governs gatekeeping of the mitochondrial Ca^{2+} uniporter. Cell Rep. 2016;14(3):403-10.

74. Patron M, Checchetto V, Raffaello A, Teardo E, Vecellio Reane D, Mantoan M, et al. MICU1 and MICU2 finely tune the mitochondrial Ca^{2+} uniporter by exerting opposite effects on MCU activity. Mol Cell. 2014;53(5):726-37.

75. Csordas G, Golenar T, Seifert EL, Kamer KJ, Sancak Y, Perocchi F, et al. MICU1 controls both the threshold and cooperative activation of the mitochondrial Ca^{2+} uniporter. Cell Metab. 2013;17(6):976-87.

76. Waldeck-Weiermair M, Malli R, Parichatikanond W, Gottschalk B, Madreiter-Sokolowski CT, Klec C, et al. Rearrangement of MICU1 multimers for activation of MCU is solely controlled by cytosolic Ca^{2+}. Sci Rep. 2015;5:15602.

77. Mallilankaraman K, Cardenas C, Doonan PJ, Chandramoorthy HC, Irrinki KM, Golenar T, et al. MCUR1 is an essential component of mitochondrial Ca^{2+} uptake that regulates cellular metabolism. Nat Cell Biol. 2012;14(12):1336-43.

78. Paupe V, Prudent J, Dassa EP, Rendon OZ, Shoubridge EA. CCDC90A (MCUR1) is a cytochrome *c* oxidase assembly factor and not a regulator of the mitochondrial calcium uniporter. Cell Metab. 2015;21(1):109-16.

79. Tomar D, Dong Z, Shanmughapriya S, Koch DA, Thomas T, Hoffman NE, et al. MCUR1 is a scaffold factor for the MCU complex function and promotes mitochondrial bioenergetics. Cell Rep. 2016;15(8):1673-85.

80. Ricquier D, Bouillaud F. The uncoupling protein homologues: UCP1, UCP2, UCP3, StUCP and AtUCP. Biochem J. 2000;345 Pt 2:161-79.

81. Trenker M, Malli R, Fertschai I, Levak-Frank S, Graier WF. Uncoupling proteins 2 and 3 are fundamental for mitochondrial Ca^{2+} uniport. Nat Cell Biol. 2007;9(4):445-52.

82. Waldeck-Weiermair M, Malli R, Naghdi S, Trenker M, Kahn MJ, Graier WF. The contribution of UCP2 and UCP3 to mitochondrial Ca^{2+} uptake is differentially determined by the source of supplied Ca^{2+}. Cell Calcium. 2010;47(5):433-40.

83. Waldeck-Weiermair M, Duan X, Naghdi S, Khan MJ, Trenker M, Malli R, et al. Uncoupling protein 3 adjusts mitochondrial Ca^{2+} uptake to high and low Ca^{2+} signals. Cell Calcium. 2010;48(5):288-301.

84. Bondarenko AI, Parichatikanond W, Madreiter CT, Rost R, Waldeck-Weiermair M, Malli R, et al. UCP2 modulates single-channel properties of a MCU-dependent Ca^{2+} inward current in mitochondria. Pflugers Arch. 2015;467(12):2509-18.

85. Socha MJ, Behringer EJ, Segal SS. Calcium and electrical signalling along endothelium of the resistance vasculature. Basic Clin Pharmacol Toxicol. 2012;110(1):80-6.

86. Ignarro LJ, Byrns RE, Buga GM, Wood KS. Endothelium-derived relaxing factor from pulmonary artery and vein possesses pharmacologic and chemical properties identical to those of nitric oxide radical. Circ Res. 1987;61(6):866-79.

87. Garland CJ, Dora KA. EDH: endothelium-dependent hyperpolarization and microvascular signalling. Acta Physiol (Oxf). 2017;219(1):152-61.

88. Palmer RM, Ferrige AG, Moncada S. Nitric oxide release accounts for the biological activity of endothelium-derived relaxing factor. Nature. 1987;327(6122):524-6.

89. da Silva CG, Specht A, Wegiel B, Ferran C, Kaczmarek E. Mechanism of purinergic activation of endothelial nitric oxide synthase in endothelial cells. Circulation. 2009;119(6):871-9.

90. Esposito B, Gambara G, Lewis AM, Palombi F, D'Alessio A, Taylor LX, et al. NAADP links histamine H_1 receptors to secretion of von Willebrand factor in human endothelial cells. Blood. 2011;117(18):4968-77.

91. Derler I, Jardin I, Romanin C. Molecular mechanisms of STIM/Orai communication. Am J Physiol Cell Physiol. 2016;310(8):C643-62.

92. Wu S, Moore TM, Brough GH, Whitt SR, Chinkers M, Li M, et al. Cyclic nucleotide-gated channels mediate membrane depolarization following activation of store-operated calcium entry in endothelial cells. J Biol Chem. 2000;275(25):18887-96.

93. Chai Q, Wang XL, Zeldin DC, Lee HC. Role of caveolae in shear stress-mediated endothelium-dependent dilation in coronary arteries. Cardiovasc Res. 2013;100(1):151-9.

94. Fulton D, Gratton JP, McCabe TJ, Fontana J, Fujio Y, Walsh K, et al. Regulation of endothelium-derived nitric oxide production by the protein kinase Akt. Nature. 1999;399(6736):597-601.

95. Lee HC. Cyclic ADP-ribose and nicotinic acid adenine dinucleotide phosphate (NAADP) as messengers for calcium mobilization. J Biol Chem. 2012;287(38):31633-40.

96. Kohler R, Brakemeier S, Kuhn M, Degenhardt C, Buhr H, Pries A, et al. Expression of ryanodine receptor type 3 and TRP channels in endothelial cells: comparison of *in situ* and cultured human endothelial cells. Cardiovasc Res. 2001;51(1):160-8.

97. Fulton D, Gratton JP, Sessa WC. Post-translational control of endothelial nitric oxide synthase: why isn't calcium/calmodulin enough? J Pharmacol Exp Ther. 2001;299(3):818-24.

98. Heiss EH, Dirsch VM. Regulation of eNOS enzyme activity by posttranslational modification. Curr Pharm Des. 2014;20(22):3503-13.

99. Chen Z, Peng IC, Cui X, Li YS, Chien S, Shyy JY. Shear stress, SIRT1, and vascular homeostasis. Proc Natl Acad Sci U S A. 2010;107(22):10268-73.

100. Michell BJ, Chen Z, Tiganis T, Stapleton D, Katsis F, Power DA, et al. Coordinated control of endothelial nitric-oxide synthase phosphorylation by protein kinase C and the cAMP-dependent protein kinase. J Biol Chem. 2001;276(21):17625-8.

101. Dedkova EN, Ji X, Lipsius SL, Blatter LA. Mitochondrial calcium uptake stimulates nitric oxide production in mitochondria of bovine vascular endothelial cells. Am J Physiol Cell Physiol. 2004;286(2):C406-15.

102. Tarpey MM, Wink DA, Grisham MB. Methods for detection of reactive metabolites of oxygen and nitrogen: *in vitro* and *in vivo* considerations. Am J Physiol Regul Integr Comp Physiol. 2004;286(3):R431-44.

103. Saldanha C, Lopes de Almeida JP, Silva-Herdade AS. Application of a nitric oxide sensor in biomedicine. Biosensors (Basel). 2014;4(1):1-17.

104. Eroglu E, Gottschalk B, Charoensin S, Blass S, Bischof H, Rost R, et al. Development of novel FP-based probes for live-cell imaging of nitric oxide dynamics. Nat Commun. 2016;7:10623.

105. Charoensin S, Eroglu E, Opelt M, Bischof H, Madreiter-Sokolowski CT, Kirsch A, et al. Intact mitochondrial Ca^{2+} uniport is essential for agonist-induced activation of endothelial nitric oxide synthase (eNOS). Free Radic Biol Med. 2017;102:248-59.

106. Edgell CJ, McDonald CC, Graham JB. Permanent cell line expressing human factor VIII-related antigen established by hybridization. Proc Natl Acad Sci U S A. 1983;80(12):3734-7.

107. Palmer AE, Giacomello M, Kortemme T, Hires SA, Lev-Ram V, Baker D, et al. Ca^{2+} indicators based on computationally redesigned calmodulin-peptide pairs. Chem Biol. 2006;13(5):521-30.

108. Bondarenko AI, Jean-Quartier C, Parichatikanond W, Alam MR, Waldeck-Weiermair M, Malli R, et al. Mitochondrial Ca^{2+} uniporter (MCU)-dependent and MCU-independent Ca^{2+} channels coexist in the inner mitochondrial membrane. Pflugers Arch. 2014;466(7):1411-20.

109. Madreiter-Sokolowski CT, Klec C, Parichatikanond W, Stryeck S, Gottschalk B, Pulido S, et al. PRMT1-mediated methylation of MICU1 determines the UCP2/3 dependency of mitochondrial Ca^{2+} uptake in immortalized cells. Nat Commun. 2016;7:12897.

110. Waldeck-Weiermair M, Bischof H, Blass S, Deak AT, Klec C, Graier T, et al. Generation of red-shifted cameleons for imaging Ca^{2+} dynamics of the endoplasmic reticulum. Sensors (Basel). 2015;15(6):13052-68.

111. Roe MW, Lemasters JJ, Herman B. Assessment of Fura-2 for measurements of cytosolic free calcium. Cell Calcium. 1990;11(2-3):63-73.

112. Scaduto RC, Jr., Grotyohann LW. Measurement of mitochondrial membrane potential using fluorescent rhodamine derivatives. Biophys J. 1999;76(1 Pt 1):469-77.

113. Harris MB, Ju H, Venema VJ, Liang H, Zou R, Michell BJ, et al. Reciprocal phosphorylation and regulation of endothelial nitric-oxide synthase in response to bradykinin stimulation. J Biol Chem. 2001;276(19):16587-91.

114. Zaobornyj T, Ghafourifar P. Strategic localization of heart mitochondrial NOS: a review of the evidence. Am J Physiol Heart Circ Physiol. 2012;303(11):H1283-93.

115. Nazarewicz RR, Zenebe WJ, Parihar A, Parihar MS, Vaccaro M, Rink C, et al. 12(S)-hydroperoxyeicosatetraenoic acid (12-HETE) increases mitochondrial nitric oxide by increasing intramitochondrial calcium. Arch Biochem Biophys. 2007;468(1):114-20.

116. Ghafourifar P, Parihar MS, Nazarewicz R, Zenebe WJ, Parihar A. Detection assays for determination of mitochondrial nitric oxide synthase activity; advantages and limitations. Methods Enzymol. 2008;440:317-34.

117. Villanueva C, Giulivi C. Subcellular and cellular locations of nitric oxide synthase isoforms as determinants of health and disease. Free Radic Biol Med. 2010;49(3):307-16.

118. Shaul PW. Regulation of endothelial nitric oxide synthase: location, location, location. Annu Rev Physiol. 2002;64:749-74.

119. Pendin D, Greotti E, Pozzan T. The elusive importance of being a mitochondrial Ca^{2+} uniporter. Cell Calcium. 2014;55(3):139-45.

120. Rimessi A, Giorgi C, Pinton P, Rizzuto R. The versatility of mitochondrial calcium signals: from stimulation of cell metabolism to induction of cell death. Biochim Biophys Acta. 2008;1777(7-8):808-16.

121. Denton RM. Regulation of mitochondrial dehydrogenases by calcium ions. Biochim Biophys Acta. 2009;1787(11):1309-16.

122. Valdez LB, Zaobornyj T, Boveris A. Mitochondrial metabolic states and membrane potential modulate mtNOS activity. Biochim Biophys Acta. 2006;1757(3):166-72.

123. Lacza Z, Pankotai E, Busija DW. Mitochondrial nitric oxide synthase: current concepts and controversies. Front Biosci (Landmark Ed). 2009;14:4436-43.

124. Valdez LB, Boveris A. Mitochondrial nitric oxide synthase, a voltage-dependent enzyme, is responsible for nitric oxide diffusion to cytosol. Front Biosci. 2007;12:1210-9.

125. Dimmeler S, Fleming I, Fisslthaler B, Hermann C, Busse R, Zeiher AM. Activation of nitric oxide synthase in endothelial cells by Akt-dependent phosphorylation. Nature. 1999;399(6736):601-5.

126. Takahashi S, Mendelsohn ME. Synergistic activation of endothelial nitric-oxide synthase (eNOS) by HSP90 and Akt: calcium-independent eNOS activation involves formation of an HSP90-Akt-CaM-bound eNOS complex. J Biol Chem. 2003;278(33):30821-7.

127. Chen ZP, Mitchelhill KI, Michell BJ, Stapleton D, Rodriguez-Crespo I, Witters LA, et al. AMP-activated protein kinase phosphorylation of endothelial NO synthase. FEBS Lett. 1999;443(3):285-9.

128. Bauer PM, Fulton D, Boo YC, Sorescu GP, Kemp BE, Jo H, et al. Compensatory phosphorylation and protein-protein interactions revealed by loss of function and gain of function mutants of multiple serine phosphorylation sites in endothelial nitric-oxide synthase. J Biol Chem. 2003;278(17):14841-9.

APPENDIX

List of publications

The key finding of the dissertation work was published in science citation index (SCI)-listed journal, according to the Dr.scient.med Curriculum Version 14.

Charoensin S, Eroglu E, Opelt M, Bischof H, Madreiter-Sokolowski CT, Kirsch A, Depaoli MR, Frank S, Schrammel A, Mayer B, Waldeck-Weiermair M, Graier WF, Malli R. Intact mitochondrial Ca^{2+} uniport is essential for agonist-induced activation of endothelial nitric oxide synthase (eNOS). Free Radic Mol Med 2017;102:248-59.

The additional side-project was part of the previously-published work, with which the doctoral student was a co-author.

Eroglu E, Gottschalk B, **Charoensin S**, Blass S, Bischof H, Rost R, Madreiter-Sokolowski CT, Pelzmann B, Bernhart E, Sattler W, Hallström S, Malinski T, Waldeck-Weiermair M, Graier WF, Malli R. Development of novel FP-based probes for live-cell imaging of nitric oxide dynamics. Nat Commun 2016;7:10623.